Univerzitet u Sarajevu
Prirodno-matematički fakultet
Odsjek za fiziku
II ciklus studija – Opći smjer – Medicinska radijaciona fizika

TESTING OF STRIPPING FOILS FOR A LIGHT ION THERAPY FACILITY

TESTIRANJE FOLIJA ZA SKIDANJE ELEKTRONA NAMIJENJENIH ZA RADIOTERAPIJSKI UREĐAJ KOJI KORISTI LAKE JONE

ZAVRŠNI – MAGISTARSKI RAD

Mentori:
prof. dr. Adnan Beganović
dr. Mariusz Sapinski

Kandidatkinja:
Amra Ibrahimović

Sarajevo, mart 2020.

Posebnu zahvalnost dugujem svojim mentorima prof. dr. Adnanu Beganoviću i dr. Mariuszu Sapinskom na predloženoj temi i izuzetnoj podršci pri izradi ovog magistarskog rada. Također, veliku zahvalu dugujem gospodinu Edmondu Offermannu koji mi je omogućio saradnju sa CERN-om, jer mi je ta saradnja omogućila izradu ovog rada.

I wish to express my deepest gratitude to my mentors prof. Adnan Beganović, PhD, and Mariusz Sapinski, PhD, for the proposed subject and their exceptional support during the development and writing of this thesis. Also, I would like to express my appreciation to Mr. Edmond Offermann who provided the opportunity to collaborate with CERN which allowed me to create this thesis.

Contents

List of Figures

List of Tables

Abstract

Hadrontherapy is a radiotherapy modality based on radiobiological properties of accelerated ions. It uses beams of particles produced by a source which is then processed until the required and optimal conditions are met. The processed beam is then finally delivered to the patient. One typical hadrontherapy facility is often quite large hosting a wide range of individual devices needed to produce an efficient beam. These include an ion source, an injector linear accelerator, a synchrotron and a transfer line that delivers the beam to the patient. The stripping foil is placed inside the injector linac and is used for the electron stripping of ions.

Amorphous carbon or carbon-based stripper foils are commonly installed in linear accelerators. Thin carbon stripper foils provide an option for directly delivering ions of required final charge states to the heavy ion synchrotron in order to mitigate space charge limitations during high-intensity operations. High beam intensities and a pulsed beam structure pose new challenges to the stripper foils which experience enhanced degradation by radiation damage, thermal effects, and stress waves. In order to ensure reliable accelerator operation, radiation-hard stripper foils are required.

This thesis discusses the stripping process by the amorphous carbon stripping foils needed to produce a charged particle beam. More precisely, this thesis is focused on the testing of the amorphous carbon stripping foils used in light ion therapy facilities. The factors that cause foil damage are also discussed. Special focus is placed on ion-beam induced structure and physical property changes, and on the influence of different beam parameters. Calculations and simulations were performed by MATLAB, Gnuplot, SRIM and LISE++ programs.

The results of the simulations, calculations and the data analysis have shown that carbon based stripping foils are very efficient and durable. The stripping process may be considered efficient after 4 MeV/u energies for all relevant ions for medical purposes.

Sažetak

Hadronska terapija je vrsta radioterapije koja je bazirana na radiobiološkim osobinama ubrzanih jona. U njoj se koriste snopovi čestica koji su proizvedeni izvorom jona, te se nakon toga procesuiraju dok se ne ispune traženi i optimalni uvjeti. Željeni snop se nakon toga dostavlja pacijentu. Tipični uređaj za hadronsku terapiju je izuzetno velik i sastoji se od velikog broja uređaja koji su potrebni za proizvodnju efikasnog snopa. To uključuje izvor jona, linerani akcelerator koji služi za injekciju snopa u sinhrotron, sinhrotron i linija transfera za dostavljanje snopa do pacijenta. Folije za skidanje elektrona su postavljene unutar alkceleratora za injekciju i namjenjene su za otklanjanje elektrona da bi se snop doveo do željenog naboja.

Folije od amorfnog karbona ili folije bazirane na karbonu su najčešće postavljene u linearnim akceleratorima. To su veoma tanke folije koje omogućavaju direktno dostavljanje jona željenog krajnjeg naboja u sinhrotron za ubrzavanje teških čestica. Snopovi visokih intenziteta i pulsirajući snopovi predstavljaju nove izazove folijama koje doživljavaju pojačanu degradaciju tokom oštećenja zračenjem, toplotnim efektima i drugim procesima kojim se opterećuju. Da bi se osigurao pravilan rad akceleratora zahtjevaju se folije otporne na zračenje.

U ovom radu su diskutovani procesi skidanja elektrona pomoću folija od amorfnog karbona potrebnih za proizvodnju snopa naelektrisanih čestica. Mnogo preciznije, u ovom radu je u fokus stavljeno testiranje folija od amorfnog karbona koji se koriste u terapijskim uređajima. Također, diskutovane su i štete koje nastaju. Posebna pažnja posvećena je strukturnim i fizikalnim promjenama izazvanim snopom naelektrisanih čestica i na uticaj različitih parametara snopa. Proračuni i simulacije su izvršene sa MATLAB, Gnuplot, SRIM i LISE++ programima.

Rezultati simulacija, proračuna i analize podataka pokazuju da su folije za skidanje elektrona bazirane na karbonu veoma efikasne i durabilne. Proces skidanja elektrona može se smatrati efikasnim iznad energija 4 MeV/u za sve vrste jona koji su relevantni za medicinsku primjenu.

Chapter 1

Introduction

1.1. What is hadron therapy

Radiotherapy is one of the most widely used therapies for cancer treatment. It consists of using radiation in different forms (X-rays, gamma rays, particles) to harm and destroy tumors. Radiotherapy can be used alone or in combination with surgery or chemotherapy. Radiotherapy can be external (teletherapy) or internal (brachytherapy).

Today, hadrontherapy is a radiotherapy procedure based on radiobiological properties of accelerated ions. The technology used in hadrontherapy develops very rapidly and is more and more available.

The word hadrontherapy implies all forms of therapeutic procedures which use a variety of beams including neutron, proton, helium ion (alpha particles), lithium ion, carbon ion, oxygen ion and other types of ion beams. Also, other terms such as “Hadron therapy”, “particle therapy”, “heavy-ion therapy” and “light ion therapy” can be used. Neutrons were the first hadrons used in therapy, however treatments with neutrons are no longer performed [1].

1.2. History

1.2.1. Conventional teletherapy

The first type of teletherapy used X-rays. During research scientists have discovered that higher energy X-rays spared surrounding tissues more in com-

parison to lower energy radiation. Because of that, scientists have developed machines which can produce higher energy X-rays. The first electron linear accelerator (linac) with energies above 1 MeV was built in the '50s at the Stanford University by Bill Hansen. Today about 20,000 linacs are installed in hospitals all over the world. There is one linac for every 170,000 – 200,000 inhabitants in developed countries.

Rapid development was caused by the development of computer assisted treatment systems and imaging technologies, such as Computed Tomography (CT), Magnetic Resonance Imaging (MRI), Single Photon Emission Computed Tomography (SPECT) and Positron Emission Tomography (PET) imaging. These techniques were implemented and combined with radiation therapy which allowed for modern and sophisticated radiation methods such as Intensity Modulated Radiation Therapy (IMRT) and Image Guided Radiation Therapy (IGRT). More recently, Volumetric Modulated Arc Therapy (VMAT) has become a powerful new tool in the hands of radiation oncologists.

Ernest Lawrence initiated hadrontherapy in 1930 with the construction of the cyclotron, and with his brother John (who was a doctor at Yale) started the idea of using accelerators in medicine. They used fast neutrons but the result of this first clinical research was not encouraging [1].

1.2.2. The beginnings of therapy with charged particles

The original idea of using proton beams in radiation oncology was suggested by Wilson in 1946. The reason for this was researching and measuring the depth profiles in the Berkeley Cyclotron. They recognized the so-called Bragg peak which had been observed 50 years before or, more precisely, in 1903. Because of the Bragg peak we can spare healthy tissues better than with X-rays. In 1954, the first patient was treated at Berkeley with protons, followed by helium treatment in 1957 and neon ions in 1975. During these treatments the beam was distributed over the target using passive shaping systems, such as scatterers, compensators and collimators that were adapted from the conventional photon therapy [1].

1.2.3. The Harvard Cyclotron

Harvard University built the first machine in 1937. During the Second world war this machine was moved to Los Alamos and used in research related to the nuclear weapons (project Manhattan) to design the first atomic bombs. Hymer

Table 1.1: The pioneers in protontherapy

Facility	Country	Year
Lawrence Berkley Laboratory	USA	1954
Uppsala	Sweden	1957
Harvard Cyclotron Laboratory	USA	1961
Dubna	Russia	1964
Moscow	Russia	1969
St. Petersburg	Russia	1975
Chiba	Japan	1979
Tsakuba	Japan	1983
Paul Scharrer Institute	Switzerland	1984

Friendell, a radiation therapist arrived at Harvard to request the movement of the machine for what he claimed were medical purposes. After the war a new cyclotron was constructed at the Harvard University and used for hadron therapy.

One young neurosurgeon from Massachusetts General Hospital in Boston, used the Harvard beam in 1961 to treat a malignant brain tumor. The early work was limited due to the inability to perform 3-D imaging and its reliance on facilities primarily dedicated to physics research.

With the development of the CT scanner, improved target definition allowed for the treatment of almost any site in the body. The subsequent development of MRI, SPECT and PET scanning has further improved target definition and allows for even more benefits of hadron therapy in general [1].

1.2.4. From Harvard to Loma Linda

In a very short time after the start-up of the Harvard facility, nuclear physics laboratories from different countries set up horizontal proton beams for therapy. Table 1.1 shows the list of facilities that used proton therapy. The important fact is that all these facilities were located in physics laboratories and that the conditions of irradiation were very far from ideal.

The first hospital-based center was built in the Loma Linda University Center in California and the first patient was treated in 1990.

In 1983 the University of Tsukuba in Japan started proton clinical studies using a synchrotron which was constructed for studies at the High Energy Accelerator Research Organization. At this facility, between 1983 and 2000, 700 patients were treated. The new facility was constructed in 2000 under the name Proton Medical Research Center and it was equipped with a synchrotron and two

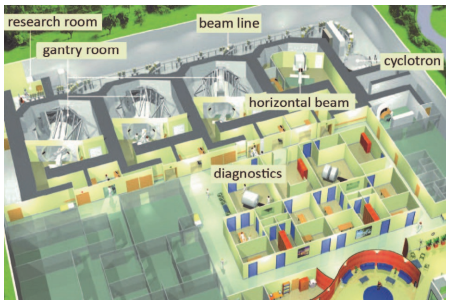

(a) Layout of a commercial proton therapy center based on a 230 MeV cyclotron featuring three gantries and a horizontal fixed beam

(b) The Bevalac was a complex formed of a linear accelerator (SuperHILAC) and a synchrotron (Bevatron) connected by a long beam transport line

Figure 1.1: Examples of hadrontherapy centers

rotating gantries. This clinical center started with treatments in September of 2001 and till March 2007, 1046 patients had been treated.

Figure 1.1 shows the examples of hadron therapy centers [1].

1.2.5. The beginnings of light-ion therapy

Helium came into use in 1957 followed by argon in 1975 both of them in Berkeley. The basic purpose of these ions was to treat different types of tumors as well as hypoxic (see Section 1.8.4) and otherwise radioresistant tumors. After argon and helium, some other ions such as silicon and neon came into use.

The first application of carbon ions was in Japan (Figure 1.2). In 1994 the Heavy Ion Medical Accelerator in Chiba (HIMAC) treated its first patient with a carbon ion beam and by the end of 2014 about 9000 patients have been treated and it has shown that many difficult and common tumors (e.g. lung and liver) can be controlled.

As of today, six centers exist in Japan and two in China [1].

1.2.6. Light-ion therapy in Europe

In Europe, the first treatment with carbon ions has been performed in the German heavy ion research laboratory GSI in Darmstadt. During the research program in the years 1997 – 2008, 450 patients were treated with a high success rate. Therefore, the decision was made to construct a dedicated treatment

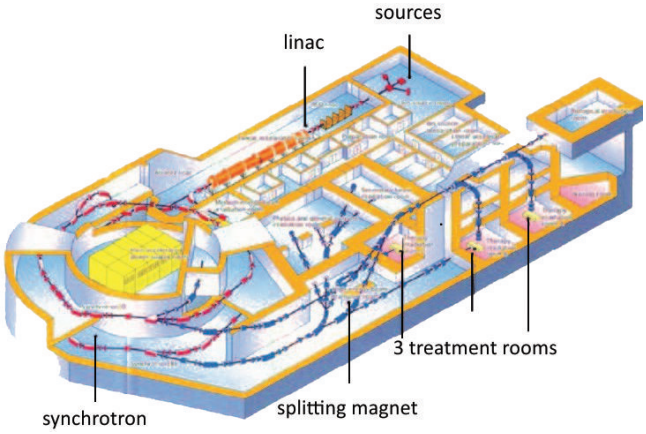

Figure 1.2: Heavy Ion Medical Accelerator in Chiba [1]

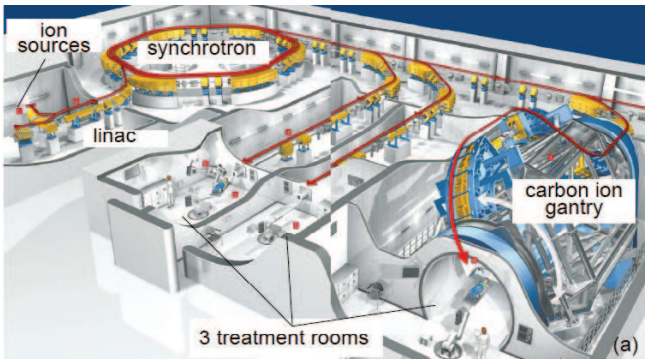

Figure 1.3: Heidelberg Ion Beam Therapy Center (HIT) features two horizontal beams and a carbon ion gantry

facility in the German Cancer Research Clinic in Heidelberg. This was called the "pilot project" and the patient treatment was moved to Heidelberg.

In November 2009 the Heidelberg Ion Beam Therapy Center (HIT) started with patient treatment and until 2014 about 1800 patients had been treated with carbon ions. On Figure 1.3 we can see how HIT looks. The gantry for carbon ions is 25 m long and weighs 700 tons, which is the first ever ion gantry. Based on HIT experience another center was constructed in Marburg, Germany.

Independently of German efforts, the Proton Ion Medical Machine Study (PIMMS) program has been started at the European Organization for Nuclear Research (CERN). Based on this, with different design, two centers were constructed CNAO and MedAustron. CNAO is a facility in Pavia which started in September of 2011 and it has proton and carbon ion treatment. In 2007, the construction of MedAustron initiated in Wiener Neustadt (Austria). The center consists

of three horizontal beams, a vertical beam, a proton gantry and the synchrotron. The first patient treatment was at the end of 2015.

European laboratories and centers have investigated the efficiency of oxygen ions (O^{8+}) and carbon ions (C^{6+}) and current results suggests that carbon ions are more efficient than oxygen ions [1].

1.3. Charged particles in electromagnetic fields

Accelerators are devices which use electric and magnetic fields to control particle beams. Therefore, this Chapter contains a short summary of basic physics laws concerning the interaction of charged particles with those fields. In accelerators an electric field is used for the acceleration of charged particles, while a magnetic field is used to guide and bend the trajectory of the particles.

A particle that has a charge q and is in an electric field $\vec{E}$ will experience directional Coulomb force $\vec{F}$:

$$\vec{F} = q\vec{E}. \tag{1.1}$$

A particle will be accelerated in a direction that depends on the sign of the charge. For example, positive charge will accelerate in the direction of electric field vector and negative in opposite direction. The velocity v that the particle has acquired can be expressed as:

$$v = \sqrt{2q|E|m}, \tag{1.2}$$

where m is the mass of the particle and $|E|$ is the magnitude of the electric field whose polarity can be neglected. By increasing the particle's velocity the kinetic energy will also increase and it can be expressed as:

$$E_{\mathrm{k}} = \frac{1}{2}mv^2. \tag{1.3}$$

When charged particles go through a magnetic field they sense the Lorentz force which is proportional to their velocities F_{L}

$$\vec{F_L} = q(\vec{v} \times \vec{B}), \tag{1.4}$$

where B is the magnetic field. When the magnetic field is perpendicular to the particle path then the magnetic force will be orthogonal to the magnetic field and to the velocity. This situation is presented on Figure 1.4. Centripetal force creates circular motion and in this case the centripetal force is the Lorentz force

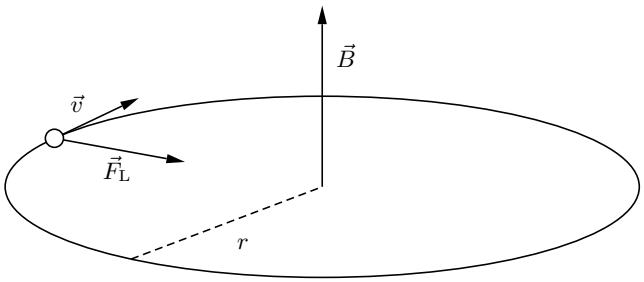

Figure 1.4: The motion of a charged particle in magnetic field

F_L . This allows centripetal acceleration which is necessary to keep the particles moving in a circular accelerator.

$$\vec{F_L} = \frac{mv^2}{r}, \tag{1.5}$$

where r is the radius of curvature. Thus:

$$qvB = \frac{mv^2}{r}, \tag{1.6}$$

and:

$$\frac{qB}{m} = \frac{v}{r} = \omega_c, \tag{1.7}$$

where ω_c is the Larmor frequency.

The cyclotron frequency f_c at which the particle completes a circular path is:

$$f_c = \frac{\omega_c}{2\pi} = \frac{v}{2\pi r} = \frac{Bq}{2\pi m}, \tag{1.8}$$

or it can be written as:

$$Br = \frac{mv}{q} = \frac{p}{q}, \tag{1.9}$$

where p is the momentum mv.

Br is the magnetic rigidity which is a measure of how much the particle is resistant to bending in the magnetic field. For example a 2 times stronger magnetic field is needed to keep a carbon ion on orbit with respect to the proton because the mass of the carbon ion is 12 times the mass of a proton and the charge is 6 times higher.

Relativistic effects

If a particle's velocity is close to the speed of light then there needs to be a relativistic correction to the laws of motion. This is done by introducing the parameters beta and gamma. The parameters beta β and gamma γ are defined as:

$$\beta = \frac{v}{c} \qquad \gamma = \frac{1}{\sqrt{1 - (\frac{v}{c})^2}} \tag{1.10}$$

where v is the particle velocity and c is the speed of light ($c = 3 \times 10^8 \, \frac{\mathrm{m}}{\mathrm{s}}$)

When particles are relativistic all their dynamic parameters are relativistic such as kinetic energy, momentum, the total particle energy etc. The total energy of a particle is given by $E = \gamma mc^2$ and the kinetic energy is given by $E_\mathrm{k} = E - mc^2$, while the particle's momentum and rigidity are:

$$p = \beta\gamma mc \qquad Br = \frac{p}{q} = \frac{\beta\gamma mc}{q}, \tag{1.11}$$

When the parameter beta is $\beta \ll 1$ then the particle isn't relativistic [2].

1.3.1. Radiofrequency acceleration

The use of electric fields is the most efficient known method to accelerate charged particles. The device in which the electromagnetic energy is transferred to charged particles is called a radiofrequency (RF) cavity. Historically the first concept of a linac was by Rolf Wideroe in 1928.

When charged particles pass through the cavity they feel the force of the electric field which increases the particles energy and pushes them forwards along the accelerator. The field is radiofrequent so it means that the field changes strength during time. The frequency of the fields varies from a few megahertz to a few gigahertz. This frequency range is typical for radio waves, hence the name radiofrequency cavity. Lower frequencies are not practical because the cavities become very large and the higher frequencies are difficult to realize because it is difficult to manufacture sub-millimeter cavities. The length range of the cavities is from a few meters to a few millimeters.

The term bunched beams implies that the particles are distributed into pulses (bunches) of particles. Bunched beams are most common in modern facilities, since the radiofrequency acceleration requires bunched beam. If particles enter a radiofrequency cavity continuously then a fraction of these particles will see

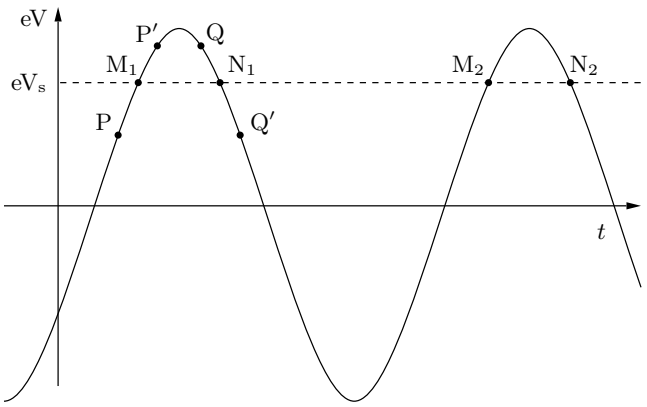

Figure 1.5: Particle phases relative to the RF field. There are equal energy gains e_{V_s} (M_1, N_1, M_2, N_2) or different energy gains (P, P′, Q, Q′) during time t

the axial field at the wrong phase during the sinusoidal time variation of the field and those particles will be deaccelerated [3, 4].

Phase stability is important for proper particle acceleration, because the field direction is not enough for stable acceleration. When two particles arrive at different times of the accelerating half period two situations are possible as illustrated on Figure 1.5. Either there are equal energy gains e_{V_s} (M_1, N_1) or different energy gains (P, P′). The particles M_1, N_1, M_2... will always see the same amplitude of the accelerating field. The particle P which arrives earlier in cavity unlike particle M_1 will get less energy and its acceleration or energy gain will be smaller and it needs more time to leave the cavity. Points M_1 and M_2 are stable while N_1 and N_2 are unstable in the sense that particles slightly away from these points will shift even more in the next gaps [5].

1.4. Magnets

As noted earlier the electric field is used to accelerate the particles while the magnetic field is used to control their trajectories. In accelerators the magnetic field is formed by different types of magnets. The system of magnets that guides and focuses a beam is called the lattice. The lattice contains dipole, quadrupole and sextupole magnets and orbit correctors. In addition the machine contains injection and extraction septa. In the following text some of these magnets, as well as their roles, will be described.

1.4.1. Dipoles

Dipole magnets consist of a north and south pole and are needed for the beam bending. The role of the dipoles is to follow the circular path which we call the 'design orbit'. By definition, this design orbit has to be a closed loop, and so the main dipole magnets in the ring have to define a full bending angle of exactly 2π.

The magnets can be made from superconductive materials. Superconducting magnets reach much higher magnetic fields than conventional iron/copper magnets at a much lower electrical power cost. They must be cooled to very low temperature, which is achieved by a continuous flow of liquid helium through the magnets or by the installation of powerful cryocoolers. Normal-conducting dipoles can generate a maximum field of 2 T, while superconducting dipole magnets in the Large Hadron Collider (LHC) reach 8.5 T [2].

1.4.2. Quadropoles

Since a beam contains a distribution of particles having different positions and angles, as well as energies, eventually the whole beam would spread out and be lost. For this reason, focusing elements are required to keep together particles with different coordinates or angles. Dipole magnets have a weak focusing effect in the horizontal plane, but a large progress occured in 1950s with discovery of strong focusing. Quadrupole magnets consist of four alternating poles which are two northern and two southern provide strong focusing [2].

Quadrupole magnets create a magnetic field that depends linearly on the distance of the particle from the design orbit:

$$B_{\mathrm{x}} = gy \qquad B_{\mathrm{y}} = gx, \tag{1.12}$$

where the constant g is called the gradient of the magnetic field and characterizes the focusing strength of the quadrupole lens in both transverse planes.

The quadrupole magnets have a special characteristic and this characteristic is that quadrupoles can behave similarly to optic lenses hence the name magnetic lenses. The magnetic lenses, same as optical lenses can be focusing and defocusing but the difference between these two types of lenses is that magnetic lenses (quadrupole) focus in one plane (say the horizontal plane) and in the same time defocus in the other (vertical) plane unlike a spherical optical lens which focuses in both planes. By constantly focusing and defocusing around the ring,

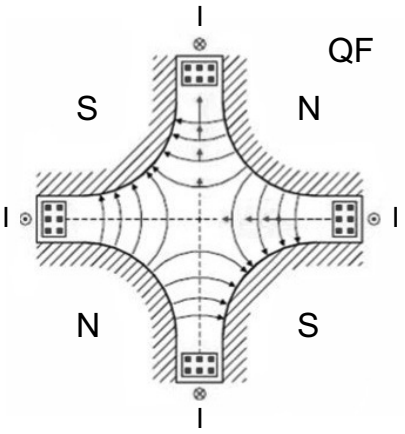

(a)

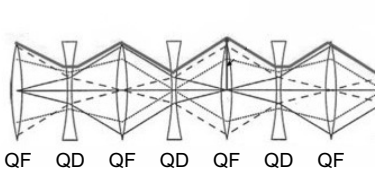

(b) QD- horizontally defocusing quadrupole; QF- horizontally focusing quadrupole

Figure 1.6: Magnetic field configuration in quadrupole magnet (left) and alternative focusing and defocusing quadrupole layout (right) [2]

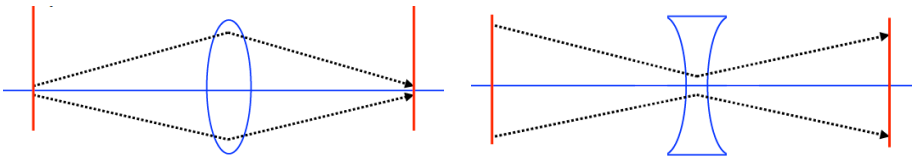

(a) Schematic illustration of the principle of the effect of a focusing quadrupole magnet

(b) Schematic illustration of the principle of the effect of a defocusing quadrupole magnet

Figure 1.7: Focusing and defocusing quadrupole magnet [6]

it is possible to keep the transverse size of the particle bunch small. Since, the magnetic lenses have the characteristic of focusing and defocusing as optical, these two types of lenses share the same equation. The schematic illustration of a focusing and defocusing quadrupole magnet are shown on Figure 1.7.

The combined focal length F of a pair of lenses of focal lengths f_1 and f_2 separated by a distance d is given by

$$\frac{1}{F} = \frac{1}{f_1} + \frac{1}{f_2} - \frac{d}{f_1 f_2}, \tag{1.13}$$

If the lenses have equal and opposite focal lengths, $f_1 = -f_2$ and the overall focal length $F = f^2/d$, which is always positive. In fact, F remains positive over quite a large range of values when f_1 and f_2 have unequal values but are still of opposite sign. Thus within certain limits a series of alternating lenses will focus. Intuitively one sees that, although the beam may be defocused by

one lens, it arrives at the following lens further from the axis and is therefore focused more strongly [2, 5–7].

1.4.3. Other magnets

A sextupole is a magnet that has six poles, three of them are north and three of them are south which are arranged in a alternating manner. This type of magnets is used in particle accelerators to reduce chromaticity which is caused by the fact that the focusing of beam particles depend on their momentum spread.

Kicker magnets have very fast increasing strength and are used to divert the incoming beam to the transport line.

A septum is a electrostatic or magnetic device for deflecting a beam or part of it from its circular orbit in a synchrotron. In most machines there are usually both types of septa magnets: first electrostatic and second magnetic.

Steerers are magnet devices designed for small-angle corrections of particle beam trajectories. Their working principle is based on the deflection of charged particles in a magnetic field. They are simply small dipoles, horizontal and vertical [2].

1.5. Beam parameters

In this section the most important parameters characterizing the beam are described, but also some of the parameters, which are strictly related to the machine (lattice) are also discussed.

1.5.1. Beam energy

The beam energy is a parameter which describes the energy of single ions in the beam. It is a kinetic energy, usually expressed in units of MeV/u, where u is the number of nucleons in the ion. The typical energies produced by the ion sources are 5 – 10 keV/u. After that various acceleration schemes are used. The output energy of an injector linac is between 4 and 10 MeV/u. The final energy needed for therapy is about 120 – 430 MeV/u for carbon and 60 – 260 MeV for protons. These energies correspond to penetration depth in human tissue between 3 and 37 cm [8].

1.5.2. Beam intensity

The beam intensity in a linac is defined by the ion source. Typical commercial ECR source produced C^{4+} beam with current of 200 µA. The pulse needed for the injection to the synchrotron is about 100 µs, what correspond to 20 pC of charge or 3×10^{10} C^{4+} ions. This is more then 2×10^{10} ions required by the new hadron therapy center, but the transmission from the source to the synchrotron is usually smaller then 50%. Therefore, a stronger source, with current of about 500 µA, is planned.

1.5.3. Beam emittance

The emittance of the beam is a surface enclosed by the contour from Figure 1.8. This contour contains 95% of the particles. The distribution of the particles in the phase space is very often Gaussian, therefore the 95% of the particles are contained within 2 standard deviation from the center of the distribution. The label of the beam emittance is the Greek letter ε. At the constant energy, the area is expressed as the $\varepsilon = \int x' dx$ and it has units of π-millimetre-milliradians. Emittance defined in such a way is often called geometrical emittance.

In general, for hadron machines the emittance is conserved. This is a consequence of Liouville's theorem: "In the vicinity of a particle, the particle density in phase space is constant if the particles move in an external magnetic field or in a general field in which the forces do not depend upon velocity." Emittance is conserved if there are no dissipative processes. For instance, the interaction of the beam with material (stripper) leads to increase of the emittance. A lot of phenomena can cause non-conservation of transverse beam emittance. Some of them are multiple scattering through a thin foil, wake fields, scattering in residual gas, filamentations etc.

In linear, or circular accelerators, where the particles energy is varied the geometrical emittance is not invariant. The invariant emittance is the normalized emittance and it is defined as

$$\varepsilon_{\mathrm{N}} = \beta\gamma\varepsilon_{\mathrm{g}}, \tag{1.14}$$

where ε_{N} is the normalized emittance and ε_{g} is the geometrical emittance, while β and γ are the relativistic parameters. The normalized emittance is the quantity that stays constant during acceleration [5].

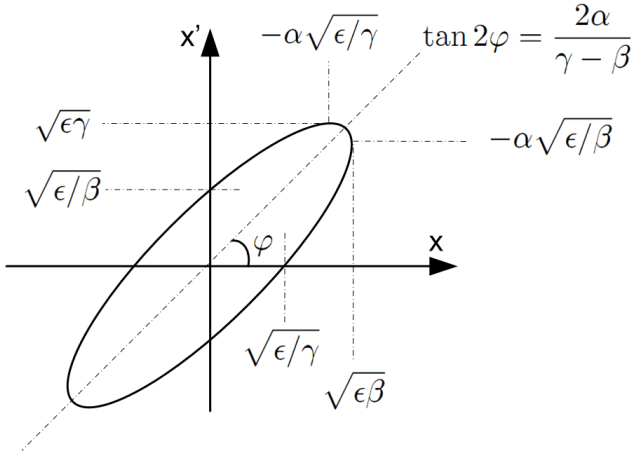

Figure 1.8: Graphical representation of the beam phase space. The Twiss parameters, alpha, beta and gamma, are most often used to describe elliptical shape of the beam phase space [9]

1.5.4. Momentum spread and dispersion

The beam is not monoenergetic, which means that it consists of a range of energies. The momentum spread is usually defined as a width of the distribution of the relative momentum variation:

$$\frac{\Delta p}{p}. \tag{1.15}$$

The typical value of momentum spread is about 10^{-3}.

The existence of momentum spread affects the particle trajectories in dipole and quadrupole magnets. This means that particles with a different momentum will be bent and focused differently [6, 10].

Dispersion represents the magnet steering error caused by different momenta of particles in the beam. It is determined by the magnetic lattice and commonly calculated using lattice design programs, like MADX [11]. In the limit of short elements the bending magnet changes the slope of the dispersion function by an amount equal to the bend angle of the magnet [12].

The dispersion function is defined by the following equation:

$$D(s) = \frac{x_i(s)}{\Delta p/p}, \tag{1.16}$$

where $x_i(s)$ is a deviation from the design orbit, s is a position along the lattice [6].

1.5.5. Beam size

The physical size of a beam dependents on the beam emittance and the Twiss parameters.

Twiss parameters

Three parameters- called Twiss (or Courant Snyder) parameters were introduced to describe the beam properties and dynamics in strong focusing machines. Those parameters are called alpha, beta and gamma. They are related to the beam shape in phase space as shown on Figure 1.8 [6].

The beta function is usually the most important of the Twiss parameters, mainly because it is directly related to the physical size of the beam along the accelerator, which is very often measured. The other two functions alpha and gamma, are defined as:

$$\alpha(s) = -\frac{1}{2}\beta'(s), \tag{1.17}$$

$$\gamma(s) = \frac{1+\alpha^2(s)}{\beta(s)}. \tag{1.18}$$

The Twiss parameters are usually calculated using specialized beam optics programs like MADX. In case of circular machines they are periodic functions of the lattice period.

These previously described parameters are needed for the definition of beam size, because they affect it. The beam size depends on its emittance and it changes along the accelerator according to the variation of the Twiss beta parameter and dispersion which as noted earlier depends on quadrupole settings - lattice. The beam size changes if the lattice is changed, even if the emittance stays the same [6]. The beam size σ is defined by the next equation:

$$\sigma = \sqrt{\beta\varepsilon + D^2(\frac{\Delta p}{p})^2}. \tag{1.19}$$

1.6. Accelerators

1.6.1. General definition

A machine which uses electromagnetic fields to propel charged particles to very high speeds and energies, and to make well-designed beams, is a particle acceler-

ator. On a basic level, particle accelerators produce beams of charged particles that can be used for a variety of research, industrial and medical purposes. The beam is then smashed either onto a target or against other particles circulating in the opposite direction.

There are two basic types of particle accelerators: linear accelerators and circular accelerators. Linear accelerators propel particles along a linear, or straight, beam line, while circular accelerators propel particles around a circular track, and can be circle (synchrotron) or spiral (cyclotron) trajectories.

The difference between a cyclotron and a synchrotron is that the synchrotron changes the magnetic field strength while the magnetic field strength in the cyclotron is constant. There is one more difference between a cyclotron and a synchrotron and it is that the synchrotron cannot accelerate particles from zero kinetic energy unlike the cyclotron. Hence, this is the reason why the synchrotron needs some pre-acceleration with a linac , microtron (type of particle accelerator concept originating from the cyclotron in which the accelerating field is not applied through large D-shaped electrodes) or another synchrotron. The initial value of energy is determined by the injection energy. When particles reach a certain value of energy then the acceleration procedure is finished. After this a beam can be delivered to a target or to another accelerator [13].

1.6.2. Light ion therapy center

A typical light ion therapy machine consists of an ion source, injector linac, synchrotron and transfer lines to the patient.

Ion sources

Electron Beam Ion Source (EBIS) – The principle of operation of an EBIS ion source is schematicaly shown on Figure 1.9. When an electron beam is produced it is first compressed to obtain high density by a strong solenoidal magnetic field. As the beam passes through the solenoid it is decelerated after which it is stopped in the electron collector. The trap region is made by a series of cylindrical electrodes in the main solenoid. By applying positive voltages on the end electrodes, electrostatics barriers for ions on the end of the trap region can be produced. The trap can be performed in a couple of different ways: injecting neutral gas of the desired species, with an axial injection or with trapping of singly charged ions which are produced in an external ion source. The ions are step-wise ionized during the holding inside the trap until

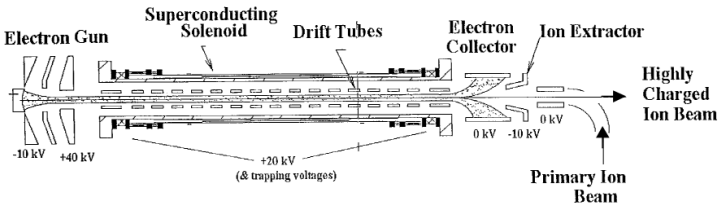

Figure 1.9: Principle of EBIS operation

they reach a certain charged state. At the same time, the voltage is reduced and the ions can be extracted. After the extraction process, the beam is delivered into the beam transport line.

An advantage of the EBIS ion source is that it can produce a narrow charge state distribution which means small beam emittance. One more advantage of the EBIS is that it can produce a fixed amount of positive charges per puls. It can be possible to increase the number of trapped charges only to the point where the electron beam space charge is neutralized [14].

Electron Cyclotron Resonance (ECR) – ECR ion sources can commonly be used as an injector into linear accelerators or can be used for the investigation and treatment of surfaces. This type of ion source has some advantages:

- It can deliver continuous beams of highly charged ions
- There are practicalIy no wearing parts that would have to be replaced from time to time and therefore it is easy to handle and can operate for very long times
- It has an excellent long-term stability and reproducibility
- It operates at pressures of about 10^{-4} mbar and therefore the material consumption is very low. This is important for the production of expensive or radioactive elements.

Electron cyclotron resonance (ECR) happens when the incident radiation with a certain frequency coincides with the natural frequency of electrons rotation in the magnetic field. The magnetic field is static and uniform and electrons inside it will move circularly because of the Lorentz force.

Electrons circular motion overlap with a uniform axial motion which results in a helix trajectory. The angular frequency of the helicoidal motion for a given

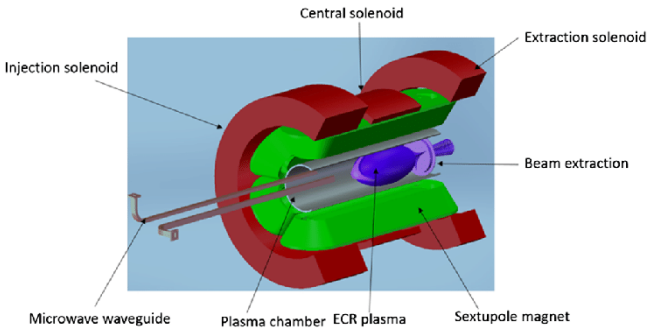

Figure 1.10: Principle of electron cyclotron resonance (ECR) operation [15]

magnetic field strength B will be:

$$\omega_{ce} = \frac{eB}{m_e}, \tag{1.20}$$

where e is the elementary charge and m_e is the mass of the electron. The characteristic of the ECR ion source is that the ECR ion source gives beams whose emittance is 5 to 10 times bigger than those of an EBIS ion source. The principle of operation of an ECR ion source is schematicaly shown on Figure 1.10. For the commonly used microwave frequency 2.45 GHz and electron charge and mass, the resonance condition is met when $B = 0.0875\,\mathrm{T}$.

$$\omega_{ce} = \frac{eB}{\gamma m_{0,e}}. \tag{1.21}$$

For particles of charge q, electron rest mass $m_{0,e}$ moving at relativistic speeds v, the equation should be adjusted according to the special relativity theory [14].

Injector linac

A linear accelerator is used to pre-accelerate ions and it accelerates the particles till their energies are in the order of a few mega-electron volts (MeV) [16].

A linear accelerator receives the particle beam from the ion source, bunches them at a requested RF frequency and then accelerates them up to the wanted energy. Injector linacs usually work in pulsed mode, which means that the cavities are powered only for a duration of puls, which is of the order of a few microseconds to milliseconds. An advantage of the linac is that particles go only once through every compound of the linac. This means that every part of the linac can be optimized for a specific particle velocity. For this reason protons and heavy ions can be accelerated with very good efficiency [8].

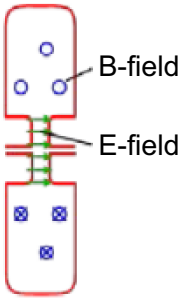

Figure 1.11: Basic accelerating cell

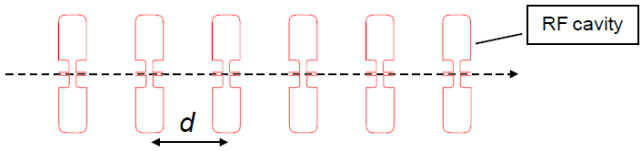

Figure 1.12: Sequence of accelerating gaps and cavities

The linac can contain a stripper foil that provides fully-stripped ions, except for argon ions that have a very low yield in getting bare nuclei [8].

An RF linear accelerator is composed of accelerating elements, and each of these elements has to generate an electric field in the region through which the beam passes. As the field oscillates, the beam particles must avoid being deccelerated, therefore the accelerating sequence is composed to drift space (usually in form of tubes) and gaps between them. The particles are screened from an electric field inside the drift spaces and accelerated in the gaps. The basic accelerating cell is shown on Figure 1.11 [16]. The example of the simplest linac structure is shown on Figure 1.12. The simplest structure contains a sequence of accelerating elements. On the figure it is assumed that all RF cavities are identical and resonate at the same angular frequency ω.

For gaining energy particles have to pass through each gap at the time when the electric field is positive i.e. the phase stability condition must be fulfilled (see Section 1.3.1). Phase stability means not only positive electric charge field, but also the right side around the maximum field, exactly as described in Section 1.3.1. The two other condition which have to be fulfilled in real accelerating structure are:

- Before the particles reach the gap sequence they must be bunched (be grouped together). The time separation between bunches must be a multiple of the RF period $T = 2\pi/\omega$

- The distances between the gaps and their relative RF phases must be correlated.

The electric field inside of i-th gap is

$$E_i = E_{0,i} cos(\omega t + \phi_i), \tag{1.22}$$

where ϕ_i is the phase of the i-th cavity with respect to a reference RF phase.

To maximize acceleration, the beam has to cross each gap at a phase ϕ_i. When particles go from one cavity to the next one, the phase has to change by an amount $\Delta\phi = \omega\tau$ where τ is the time that a particle needs to cross a distance d, but for relativistic particles, the change in phase will be:

$$\Delta\phi = \omega\tau = \omega\frac{d}{\beta c} = 2\pi\frac{d}{\beta\lambda}, \tag{1.23}$$

where β is the relativistic parameter.

To achieve acceleration the distance between gaps and phase difference between them have to be correlated and their ratio $(d/\Delta T)$ is proportional to $\beta\lambda$. In a non-relativistic case, the energy increasing means that either $\Delta\phi$ or distance d has to be changed. In other terms that means that it is needed to progressively increase the distance d or progressively decreases RF phase. This is a way to keep synchronicity between the particle beam and the accelerating wave.

It is possible to describe two types of linear accelerators i.e. the two different orders of RF cavities:
Individual-cavity linacs (Figure 1.13a) have a fixed distance between cavities, and the phase of every cavity has to be adjusted to the increase in beam velocity. Each RF cavity has to have an individual RF amplifier. This type of linac allows accelerating different particles (in different charged states or with different energies). This means that it just requires a different set of cavity phases for each ion or particle. The main disadvantage is the high cost because of the large number of RF cavities and their amplifiers.
Coupled-cell cavity linacs (Figure 1.13b) have a fixed cavity/gap and the distance between them changes according to the beam velocity. If the phase difference between the gaps is precisely defined, it is convenient to couple together some of them on a common RF power source. With this it is possible to reduce the cost of the RF system.

A linac system is made of a ion source, a bunching system (often RFQ) and a sequence of cavities (grouped or not). In order to keep the beam focused, the focusing elements (quadrupoles or solenoids) are often build around drift

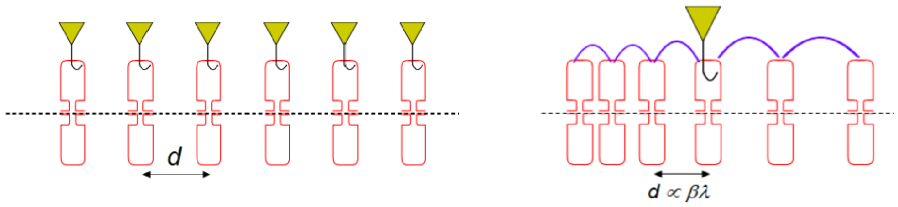

(a) Single-cavity linac (b) Coupled-cell cavity linac

Figure 1.13: Two different orders of RF cavities

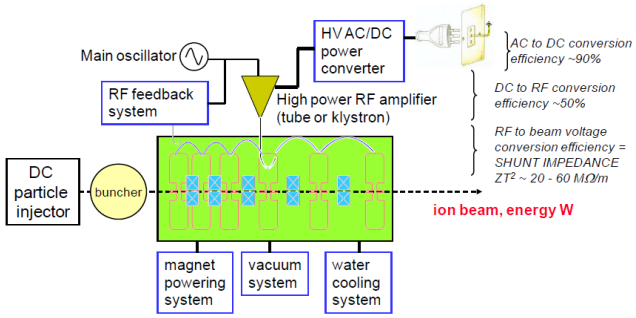

Figure 1.14: Scheme of a linac accelerating system

tubes of the linac. The cavities are powered by RF amplifiers. So, the linac must accomodate a vacuum system, a magnet powering system, a water-cooling system to evacuate the excess power which comes from the RF system and beam instrumentation.

A basic scheme for a linac accelerating system is shown on Figure 1.14 and represents how a linear acceleration system transforms the electrical energy which comes from the grid into kinetic energy of the particle beam. The transformation has some losses so the efficiency of the transformation is quite low. These losses are mainly manifested as heat dissipation in cavity walls and must be removed with the cooling system. Therefore the energy transformation passes through three steps:

- The conversion of the AC power from the grid (alternating, low voltage, high current) into DC power
- The following conversion of DC power into RF power
- The final conversion of RF power into power given to the particle beam takes place in the gap of the accelerating cavity

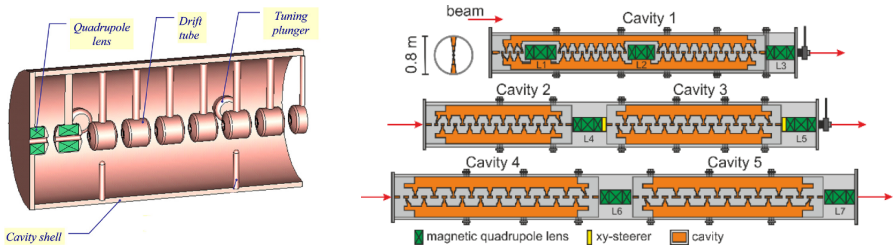

(a) DTL structure [16] (b) IH structure [17]

Figure 1.15: Different structure of linac

Below two types of linac structures used for low energy acceleration are described.

Drift tube linac(DTL)

The most important structure that works in transverse magnetic (TM) mode is the Drift Tube Linac (DTL), sometimes called the Alvarez linac. The DTL is a chain of coupled cells. The wall between the cells is completely removed in order to increase the coupling, leaving around the axis series of hollow tubes which are called drift tubes. This structure is shown on the Figure 1.15a. The high coupling allows avoiding the instabilities which can be very dangerous, even in case when the structure contains a large number of cells. Removing the walls between cells does not affect power loss because the RF currents flow only on the external tank of the tubes.

The drift tubes have two functions, the first of which is to hide the particles during the half RF period when the electric field on the axis is decelerating, and the second function is to concentrate the electric field around the gap to increase the accelerating efficiency. If the diameter of the tube is quite large it can be used as housing for the focusing quadrupoles that can keep the beam focused in the transversal plane.

An important fact is that the lenght of the cells and the drift tubes can be easily increased to follow the increase in beam velocity avoiding the frequency or the electric field distribution.

IH-structure

One of the linac types is based on the operation in a transverse electric (TE) mode. This transverse electric mode (TE) is usually called H mode. The largest part of the cavity is electric field in the transverse plane. Drift tubes are placed in the structure and connected to two sides of the resonator. The electric field in the center of the cavity is reoriented towards the beam direction and focused

allowing for high acceleration gradients in the longitudinal direction between the drift tubes and then it is possible to provide acceleration. IH structures provide a longitudinal electric field between the drift tubes as a consequence of the supports of the drift tubes which are placed on the two accelerating structures. The IH structure is very compact in terms of transverse dimensions. This structure is adequate for low frequencies but it is very complicated to construct it if the higher frequencies are requested. This structure is shown on the Figure 1.15b [16].

Synchrotron

In a synchrotron particles travel around a fixed closed orbit. The magnetic field is used for bending the particle's trajectory. During the accelerating process the strength of the magnetic field increases with time and is synchronized with the increasing kinetic energy of the particles.

The particle trajectory in the synchrotron does not depend on energy. This is only possible with magnets whose magnetic fields vary as the particles accelerate. In the synchrotron's lattice magnets are joined by field-free regions or drift space. Synchrotrons in various centers differ in the placement and position of their components. In a region of very high energies where the particle's velocity is near to the speed of light the frequency of the RF system is constant, but at lower energies which are needed for proton or light ion therapy the RF must vary in synchronization with the energy and the magnetic fields. A schematic diagram of a synchrotron is plotted on Figure 1.16. Particles are injected into the synchrotron after pre-acceleration.

There are several specialized types of synchrotron machines that are used today:

A storage ring is a type of synchrotron which is used to keep the kinetic energies of the particles constant. In it particles can be kept on circulation for many hours whether it is in pulse or continuous mode. Storage of a particle depends on the mass, momentum and usually the charge of the particle. Storage rings most commonly store electrons, positrons, or protons. An example of a storage rings is the Experimental Storage Ring (ESR) in GSI, Germany.

A synchrotron light source is a storage ring designed to generate wide-spectrum and high energy electromagnetic radiation used for further research. A synchrotron light facility often contains another synchrotron which is called a booster. The booster accelerates the beam to the final energy, so that the storage ring does not have to be ramped. Examples of synchrotron light sources are ALBA in Barcelona, Spain, European Synchrotron Radiation Facillity in

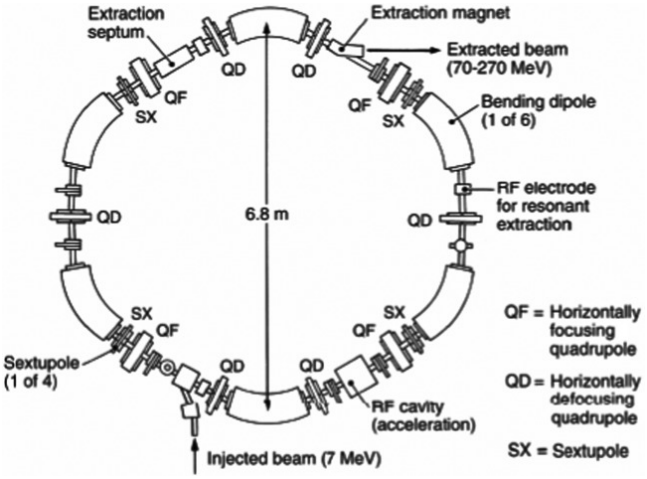

Figure 1.16: Schematic diagram of synchrotron

Grenoble, France etc. There are more than 50 synchrotron light sources in the world.

A circular collider is an accelerator which colliding two beams moving in the opposite directions. The type of particles, the energy of the collisions and the luminosity are among the important characteristics of an accelerator. Luminosity is a key indicator of a collider's performance: it indicates the number of potential collisions per surface unit over a given period of time expressed in $\frac{1}{\mathrm{cm}^2\,\mathrm{s}}$ [18].

Transfer lines

The beam is extracted from a synchrotron after reaching the desired energy or when it is not needed anymore in a collider or light source. This is done into an external beam-line and transported to a patient, experimental target or a beam dump.

The beam can be extracted in fast or slow mode. In fast extraction mode a kicker kicks the whole beam to the extraction channel, which starts with a septum magnet.

In slow extraction mode beam particles are slowly sent to the extracting channel using resonance in phase space. The resonance is done by pushing the particles out of the stable area (stable area is surrounded with unstable area) so that the particles move away and than captured by septum magnet. One of the method

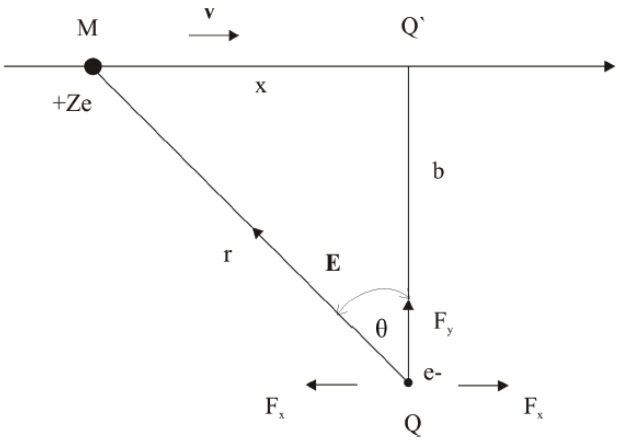

Figure 1.17: Interaction between a heavy charge particle and an electron in the point Q

used to push particles outside the stable area is excitation with transverse RF signal. This method is often used in medical machines [19].

The transfer lines are made of dipoles and quadrupoles, no RF cavities and usually no higher multipoles [2, 8].

1.7. Beam interaction with matter

When protons and ions pass through a medium, they interact predominantly with electrons present in the target via the Coulomb force. In this interaction the electrons gain energy and the projectile loses its energy. The projectiles also interact with target nuclei via Coulomb interaction leading to elastic and inelastic collisions and via nuclear interactions, in which the projectile is not only scattered and slowed down but can also be fragmented into lighter nuclei. The deviation of the projectile due to nuclear scattering is much stronger than due to interaction with electrons, but the probability of interaction with electrons is several orders of magnitudes larger.

Particles that are heavier than electrons and which are charged, of course, scatter through much smaller angles. This results in a sharper lateral distribution unlike electron or photon beams [20].

1.7.1. Energy loss - Stopping power (dE/dx)

It can be proven that the energy loss rate is proportional to the square of the particle charge and, for energies smaller than a few GeV/u inversely proportional to the square of its velocity. For energies larger then a few GeV/u the energy loss rate increases due to relativistic effects.

On Figure 1.17 a charged particle is labeled with M with velocity v and charge $+Ze$ which is moving in the direction MQ'. On the electron with mass rest m_e and with the position in point Q will affect the Coulomb force F. The Coulomb force can be presented with Equation (1.24).

$$F = k\frac{Ze^2}{r^2} \qquad k = 8.9875 \times 10^9 \,\frac{\mathrm{N\,m^2}}{\mathrm{C^2}}. \tag{1.24}$$

The Coulomb force F has two perpendicular components F_x and F_y. When a heavy particle goes through point Q', F_x doesn't affect the electron moving along the x direction. But there is F_y which always has the same direction and which initiates it. If a heavy particle has a big enough mass which is bigger than the rest mass of an electron, then the heavy particle deviates very little from the original direction of motion MQ'. The heavy particle will submit a little amount of the energy ΔE. This delivered energy can be calculated.

The momentum which will be delivered to the electron is Δp:

$$\Delta p = \int_{-\infty}^{+\infty} F_\mathrm{y}\,\mathrm{d}t = \int_{-\infty}^{+\infty} k\frac{Ze^2}{r^2} cos\theta\,\mathrm{d}t \tag{1.25}$$

Because

$$\frac{F_\mathrm{x}}{F} = cos\theta; F_\mathrm{y} = Fcos\theta = k\frac{Ze^2}{r^2}cos\theta \tag{1.26}$$

$$\frac{b}{r} = cos\theta \tag{1.27}$$

$$\frac{dx}{dt} = v \Rightarrow dt = \frac{b}{v}\frac{d\theta}{cos^2\theta} \tag{1.28}$$

Then the integral becomes

$$\Delta p = \frac{kZe^2}{bv}\int_{-\pi/2}^{+\pi/2} cos\theta d\theta = \frac{2kZe^2}{bv}, \tag{1.29}$$

where r_0 denotes the classical mechanical radius of an electron,

$$r_0 = \frac{ke^2}{m_e c^2} = 2.817\,94 \times 10^{-15}\,\mathrm{m} \tag{1.30}$$

The electron's momentum is becomes:

$$\Delta p = \frac{2Zr_0 m_e c^2}{vb}. \tag{1.31}$$

So, the energy that the particle delivers to an electron is

$$\Delta E(b) = \frac{(\Delta p)^2}{2m_e} = \frac{2Z^2 r_0^2 m_e c^4}{v^2 b^2} \tag{1.32}$$

Because a heavy particle has kinetic energy

$$E_k = \frac{1}{2} M v^2 \tag{1.33}$$

The delivered energy then becomes

$$\Delta E(b) = \frac{Z^2 r_0^2 m_e c^4}{b^2} \cdot \frac{M}{E_k}. \tag{1.34}$$

From the previous equation the fact comes up that the delivered energy $\Delta E(b)$ is inversely proportional to the kinetic energy of a heavy particle E. If a heavy particle has a large kinetic energy this implies a short time of interaction, because of high particle velocity. This short time of interaction implies a small amount of delivered energy. The second important parameter is the distance b (parameter of collisions) which is the distance that a heavy particle passes next to an electron. Since the delivered energy is inversely proportional to the distance b a closer passage of a heavy particle causes a larger loss of energy. The next part is going to show the whole amount of the heavy particle's kinetic energy which is lost by its passage through an absorber.

If the electrons are randomly distributed in an absorber's space around the particle's trajectory the number of electrons Δn in a cylindrical layer of absorber which has thickness db and length Δx will be:

$$\Delta n = N_e \rho \Delta V, \tag{1.35}$$

where N_e is a number of the electrons per mass of medium, ρ is a density of medium, and ΔV is a volume of the cylindrical layer of medium with thickness db.

The volume is:

$$\Delta V = 2\pi \Delta x \frac{2b + db}{2} \mathrm{d}b. \tag{1.36}$$

And for $b \gg db$ The volume is:

$$\frac{2b + db}{2} \approx b, \tag{1.37}$$

Then the number of electrons located in the volume ΔV of the medium is:

$$\Delta n = 2\pi N_e \rho \Delta x b \, \mathrm{d}b. \tag{1.38}$$

To find the total energy loss of on a path length Δx, it is needed to multiply the loss of the energy $\Delta E(b)$ with the number of electrons Δn in a cylinder with volume ΔV and then integrate over all the values of parameter of collisions b, from $b_{\min}$ to $b_{\max}$.

$$\frac{\mathrm{d}E}{\mathrm{d}x} = \int_{b_{\min}}^{b_{\max}} \Delta E(b) \frac{\Delta n}{\Delta x} = 4\pi N_e \rho \frac{Z^2 r_0^2 m_e c^4}{v^2} \int_{b_{\min}}^{b_{\max}} \frac{\mathrm{d}b}{b} \tag{1.39}$$

$$\frac{\mathrm{d}E}{\mathrm{d}x} = 4\pi N_e \rho \frac{Z^2 r_0^2 m_e c^2}{\beta^2} \ln \left[\frac{b_{\max}}{b_{\min}} \right] \tag{1.40}$$

When the stopping power $\mathrm{d}E/\mathrm{d}x$ is divided by the density of matter through which the particles pass the mass stopping power is obtained. The mass stopping power is energy lost per unit path length in $\mathrm{g/cm^2}$. When a particle goes through medium there is a difference in slowing down between medium with high Z and low Z. Medium with a high Z scatters particles with large angels so if it's needed to scatter a beam with minimum loss of energy it is recommended to use a material with high Z. On the other hand, if it's needed to slow down a beam with minimum amount of scattering it is recommended to use materials with low Z. The equation below shows how to calculate mass stopping power S_{ion} and it is called the Bethe-Bloch formula [20].

$$S_{\mathrm{ion}} = \frac{1}{\rho}\left(\frac{\mathrm{d}E}{\mathrm{d}x}\right) = 4\pi r_0^2 N_e \frac{Z^2 m_e c^2}{\beta^2} \left[\ln \frac{2 m_e c^2 \beta^2}{I(1-\beta^2)\beta^2} - \beta^2 - \sum_i \frac{C_i}{Z} \right], \tag{1.41}$$

where I is the average energy of excitation, C_i are coefficients which are determined experimentaly. The last part in this equation is a correction on the atomic shell and adjustment to the way of binding between the electron and the atomic shell. The whole part in the brackets behaves as a slow growing function. The conclusion is that the energy lost by the charged particle in an absorber will appear as ionizing and excitation process but not as chemical changes. Beta β is the relativistic parameter [21].

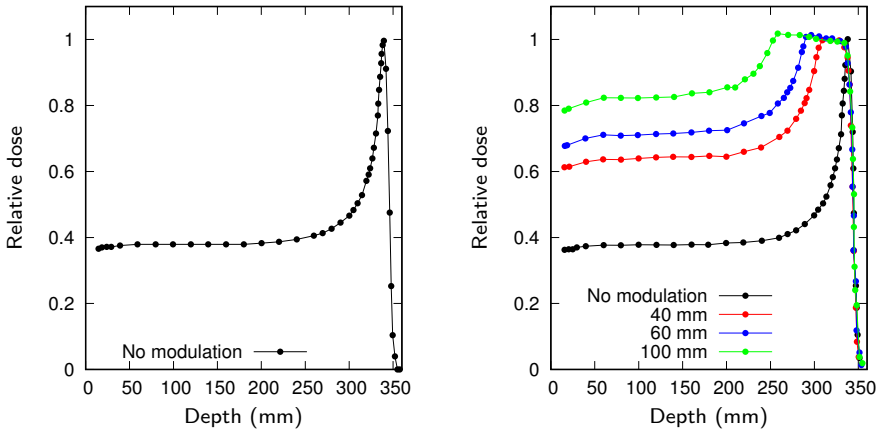

(a) Bragg peak of a proton beam (b) Spread-out Bragg peak

Figure 1.18: Bragg peak

1.7.2. Bragg peak

The ions and protons have a characteristic which plays an important role in radiotherapy, this characteristic is expressed in dose distribution. The name of the characteristic is Bragg peak which is named after Sir William Henry Bragg who investigated the energy deposition of charged particles. A depth-dose profile of heavy charged particles shows a flat plateau region with low dose and an expressive peak near to the end of the range of the particles. The average rate of energy loss of a particle per unit path length in a medium is called the stopping power.

The stopping power is the result of the interaction between particles and the medium in the slowing down process that is represented by the Bethe-Bloch formula (see Equation (1.41)). This formula shows a $1/\beta^2$ dependence of the specific energy loss. When the incident ions (projectiles) enter in a absorbing medium then an interaction starts and it is governed by inelastic collisions with the atomic electrons. During high velocities the ions lose small amounts of the kinetic energy and as the particle loses energy, it slows down and the rate of energy loss per unit path length increases. When the particle velocity approaches almost zero near the end of its range, the rate of energy loss becomes maximum and this maximum energy loss happenes when projectiles reach the Bohr velocity $v_B = \frac{e^2}{(h/2\pi)}$ [22].

The measuring unit for stopping power is MeV/cm and the label is $(-\mathrm{d}E/\mathrm{d}x)$. This can be referred to the linear energy transfer (LET) of the particle. The

stopping power and LET are very closely linked with the dose deposition in a tissue or medium through which they pass and with the RBE (see Section 1.8.3).

The Bragg peak of a monoenergetic proton beam can be seen in Figure 1.18a. Its shape is too narrow and cannot cover the extent of most target volumes. It is possible to spread out the Bragg peak using the superposition of a few beams of different energies as shown on Figure 1.18b. These beams are called the spread-out Bragg peak (SOBP). It is important to notice that on Figure 1.18a and Figure 1.18b just after the Bragg peak or SOBP the depth-dose curve drops off very fast and sharply to zero but there is a slight slope. This slight slope is caused by energy loss straggling of the particles when they are close to the end of their range [20].

1.7.3. Beam interaction with thin foils-Stripping process

When an accelerated beam goes to the stripper the beam's ions are stripped of some of their electrons and the charge state of beam particles increases. As the beam particles have larger positive charge, the energy transfer from the accelerating field to the beam is more efficient (see Equation (1.1)) and the Lorentz force for keeping beam trajectory inside the synchrotron is larger (see Equation (1.4)). The stripper is a very thin layer of matter and can be a stripping foil or gases through which the beam passes. Solid strippers must be very thin because of which they are called stripping foils. There are some differences between these types of strippers. Gas strippers can provide small multiple scattering and energy straggling. While gas strippers allow a higher average of positive charge and hence of higher output energy, foils provided a higher beam intensity which is the most important characteristic. These two types of strippers will be described in the following text [23].

Gas stripper

Argon or nitrogen gases are usually used in gas strippers and they are supplied through a bottle located in the system or a supply bottle with a regulator outside the pressure vessel. A metal metering valve is provided to dose gas to the stripping canal. One, two or three turbo-molecular pumps are provided in the terminal to allow circulation of the stripper gas, depending on the system. The turbo-pump output has a trap with the help of which it can prevent contamination of the stripper gas. Well designed pumping restrictions ensure that the pressure in the acceleration tube near the stripping place is at last 10^3 times

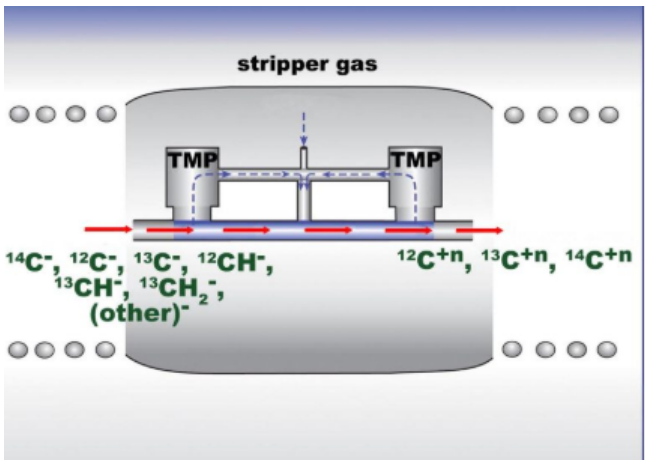

Figure 1.19: Gas stripper

lower than in the stripper canal. Figure 1.19 shows schematicaly how a gas stripper looks .

Stripping foils

Thin foils are used in many types of ion-beam accelerators . The most commonly applied are amorphous carbon based stripping foils.

With very thin thickness of stripping foils the loss of beam particles and energy is avoided but the foils must be thick enough to achieve near-equilibrium charge exchange, and to have a reasonable lifetime under beam bombardment. The rate of foil damage increases with ions mass and multiple scattering becomes important as the mass of the beam increases. Foils with a thickness of about $5\,\frac{\mu g}{cm^2}$ (ie. 250 Å or 25 nm) have provided a suitable compromise between the various factors. The lifetime of the stripping foil depends on the application and type of foil. The lifetime of a conventional stripper foil under ion beam irradiation can be from a few minutes to a few years.

Carbon stripping foils provide direct delivery of ions of the desired charge to the ion synchrotron. Sometimes, especially for heavier ions, the stripping process is done in multiple stages in order to optimize the final intensity of the beam. A second stripper might be inserted at higher beam energy and is beneficial to reduce the accelerating voltage. With a two stripper approach, linac design could be optimized in terms of compactness, efficiency, reliability and last but not least in terms of costs [24].

Figure 1.20: Carbon based stripping foils [27]

High beam intensities and pulsed beams on the stripping foils create a larger probability for radiation damage, thermal effects and stress waves. Radiation-hard stripping foils are required to ensure reliable accelerator operation. Because of different damages and changes on the foil it is possible to investigate these damages by different methods. It is possible to estimate microstructural changes, structural changes, the changes of physical properties and temperature measuring. Another way of testing is to use specific software to simulate certain damages to the stripper foils [25, 26].

Microstructural changes were investigated with various methods such as [28]:

- optical microscopy
- scanning electron microscopy (SEM)
- profilometry and chromatic aberration measurements

Structural changes were investigated with:

- X-ray photoelectron spectroscopy (XPS)
- Raman spectroscopy
- high resolution transmission electron microscopy (HRTEM)
- in-situ Fourier-transform infrared spectroscopy (FTIR)
- small angle X-ray scattering (SAXS)

The changes of physical properties can be investigated by:

- the electrical resistivity
- thermal conductivity and stiffness of the foils can be studied by an in-situ 4-point probe
- laser flash analysis

- atomic force microscopy (AFM)

Measuring temperature:

- infrared (IR) camera

Amorphous carbon stripping foils

The most common material which is used for making stripping foils is amorphous carbon. The interest in this kind of material is largely because this material has a very acceptable combination of advantages. These include beam parameters after stripping such as low energy straggling, minimization of multiple scattering and high ion beam transmission. Stripping foils provide higher charge states then gas strippers. The vacuum stability, stability at high temperatures and low long term activation are other advantages of the amorphous carbon stripping foils. These types of the foils can be produced by four metods: arc discharge, laser ablation, sputtering and ion beam deposition.

During the years scientists developed ways to extend foil lifetime. Some of them are by the doping process or mounting the foil on rotating stripper wheels to distribute the ion beam over a large area.

Carbon can be in crystalline or non-crystalline form (graphite and diamond crystal grid). The differences between these two types are interatomic distances and interbonding angles. The microstructure of carbon has three possible hybridizations sp^3, sp^2, and sp^1. Because of these three states it is versatile.

Primarily, amorphus carbon has sp^2 and sp^3 hybridizations. In the sp^3 hybridization, which is fourfold bonding configuration, the carbon atoms have a form of four tetrahedrally oriented sp^3 orbitals. This produces four strong σ (sigma) bonds. In case of sp^2 hybridization, that is threefold configuration, the carbon atoms are bonded with three σ bonds and one weaker π bond. These atoms are oriented trigonally in the way that one π orbital lies perpendicular to the sp^2 orbital plane.

The ratio and grouping of these bonding configurations strongly determines the material properties. If the strong bonds dominate ie. high content of sp^3, the amorphus carbon is more dense than the amorphus carbon with high sp^2 content. In respect to the sp^2 to sp^3 ratio, carbon can form large amounts of structures with different densities from less than $2\,\frac{g}{cm^3}$, to more than $3\,\frac{g}{cm^3}$.

The bonding ratio in amorphous carbon together with the degree and way of grouping defines the properties of the final structure. sp^3 bonding gives the

amorphous carbon mechanical hardness as well as chemical, and electrochemical inertness and optical transmittance, while the sp^2 bonding provides electrical conductivity. Tailored engineering of the microstructure can therefore access a broad spectrum of properties for special demands.

Various methods are used for the deposition of amorphous carbon films. Arc discharge, laser ablation, sputtering and ion beam deposition produce films with a high degree of sp^3 bonding while evaporated films are mainly sp^2 coordinated [28].

Stripping process

The stripping process is a process of removing electrons from partly charged ions which means changing the injected negative ions into positive ions. These positive ions can be used for different purposes, to research the characteristics of materials or to treat board types of tumors.

The process of electron loss can be shown as:

$$(P + e) - T \rightarrow P - (e - T'), \tag{1.42}$$

where P is the bare projectile nucleus, e is the electron to be stripped from the projectile ion and T is the target. The parenthesis indicates that the stripped electron can be attached to the target atom or maybe become free. The T' means that the final state represents the fact that a target atom might be in an excited state [29].

The effects of the ion stripping process on ion acceleration are two fold. On the one side, the passage of ions through stripping foil can be exploited to produce an increase of the ion charge which reduces the effective potential required for further acceleration. On the other side, good vacuum conditions allow to avoid random stripping in the residual gas of an accelerator which leads to beam losses. In order to calculate the vacuum which guarantees a satisfactory particle transmission, it is necessary to know the charge change cross sections [30].

The ion sources are more efficient in producing C^{4+} ions rather than C^{6+} ions. Fully charged ions have a maximum q/m ratio, therefore they are most efficiently accelerated in RF-cavities and have the smallest bending radius in circular machines. For example in current carbon therapy machines, the ion source produces C^{4+} ions which are completely stripped to C^{6+} before injection to the synchrotron.

A calculation of the cross-section for the stripping process implies integrating over all final states of the target and the projectile, for interjection, in which the energy transfer to the projectile's electron exceeds the electron's binding energy [29].

Estimating the charged-state of the fast projectile ions in targets is a quite complex problem. The ion suffers successive collisions with the atoms of the target, which are responsible for its slow down. The ions are exposed to different ellementary processes such as electron capture, ionization and excitation. Ionization and excitation are dominant at high velocity and then a perturbative treatment is applicable. By decreasing the ion velocity, all the processes at the end make the modeling much more complicated. By developing the ETACHA code, it is enabled to predict the evolution of ion charge-state distribution as a function of the solid target thickness for a wide range of collision velocities and by taking into account ions with up to 60 orbital states of electrons.

The calculation of ion charge-state distributions as a function of penetration depth (x) in the target is performed by solving a set of differential equations of the type:

$$\frac{\mathrm{d}Y_i(x)}{\mathrm{d}x} = \sum_j Y_j(x)\sigma_{ji} - \sum_j Y_i(x)\sigma_{ij}, \tag{1.43}$$

where $Y_i(x)$ stands for the fraction of ions in a specific i electronic configuration, and σ_{ij} for collision cross sections or transition rates from state i to state j and vice versa.

With this program it is possible to calculate stripping efficiency of different kinds of foils and different ions as projectiles.

The ETACHA code is already used by many physicists working on the production of intense multicharged ion beams at large scale facilities such as GANIL in France, GSI in Germany, Riken in Japan, Argonne National Lab in USA. For this thesis the ETACHA envoirment is used as part of the LISE++ program [31].

Consequences of the stripping process

During the interaction between the foil and the beam, different changes occur on both the foil and the beam. These changes manifest themselves as damage to the foil and a change in beam properties. The dominant process during the collision is Coulomb scattering. The consequences of this interaction are heating

the foil, moving the film atoms from their positions, inserting atoms, spreading the beam, shortening the lifetime of the foil, etc.

In the following text the estimation of changes in the beam and foil will be described. The estimations are evaluated by programs. The first consequence that will be described and explained is the change in the foil, which is the heating of the foil, ie. the temperature increase of the foil.

The increase of the foil temperature can be calculated by the following equation :

$$\frac{\mathrm{d}E}{\mathrm{d}x}N = \rho V c_p \Delta T, \tag{1.44}$$

where $\mathrm{d}E/\mathrm{d}x$ is a stopping power of certain ions in the foil, N is the number of ions, ρ is the foil density, V is the foil volume, c_p is specific heat capacity and ΔT is a temperature increase. This equation doesn't consider the cooling effects because the estimated temperature increases are very low and cooling is important for high temperatures.

The following changes are some of the possible types of radiation damages that can occur on the foils during the stripping process. Displacement is the process where an energetic incident atom knocks a lattice atom off its site. Vacancy is an empty lattice site (without an atom). Originally all lattice sites are occupied, and displacements cause vacancies. Interstitial Atoms are atoms which were knocked out of their original site, and came to a stop in the foil. Also the incident ions, when they stop, are considered interstitial atoms. Replacement collisions occur when an foil atom is replaced with an identical atom. This is the only mechanism in which a vacancy may be re-occupied. Displacement Energy is the minimum energy required to knock a target atom far enough away from its lattice. This minimum energy produces a "Frenkel Pair" which is a single vacancy and a nearby interstitial atom, which is the most fundamental type of damage caused by an ion. It takes energy to break electronic bonds and displace an atom from a lattice site. Surface Binding Energy is when an atom at the target surface is not confined on one side, so the energy required to remove it from its lattice site is less than if it was inside the solid and surrounded by other atoms. A surface atom has fewer electronic bonds which too must be broken. This energy is especially important for calculating sputtering (removal of surface atoms).

Displacement per atom (dpa) is a parameter that shows a mechanical failure of the target. The failure occurs at 0.1 to 2 dpa.

Assume an incident atom has an atomic number Z_1, and energy E. It has a collision within the target with an atom of atomic number Z_2. After the collision, the incident ion has energy E_1 and the struck atom has energy E_2.

An Atomic Displacement occurs if $E_2 > E_{\text{disp}}$ (the hit atom is given enough energy to leave the site). A vacancy occurs if both $E_1 > E_{\text{disp}}$ and $E_2 > E_{\text{disp}}$ (both atoms have enough energy to leave the site), and both atoms then become moving atoms. If $E_2 < E_{\text{disp}}$ then the struck atom does not have enough energy and it will vibrate back to its original site releasing E_2 as phonons (energy deposited into crystal lattice vibrations)

If $E_1 < E_{\text{disp}}$ and $E_2 > E_{\text{disp}}$ and $Z_1 = Z_2$, then the incoming atom will remain at the site and the collision is called a replacement collision with E_1 released as phonons. The atom in the lattice site remains the same atom by exchange. This type of collision is common in single element targets with large recoil events. If $E_1 < E_{\text{disp}}$ and $E_2 > E_{\text{disp}}$ and $Z_1 \neq Z_2$, then Z_1 becomes a stopped interstitial atom. If $E_1 < E_{\text{disp}}$ and $E_2 < E_{\text{disp}}$ then Z_1 becomes an interstitial and $E_1 + E_2$ is released as phonons.

The sums of these damage types are related with two following expressions:

Displacements = Vacancies + Replacement Collisions
Vacancies + Replacements = Interstitials + (Atoms which leave the target volume)

The damages, which occur on the foil, affect the foil lifetime and its durability. So, the following equation is used to estimate the lifetime of the foil.

$$t = \frac{E_{\text{disp}} M_2 E}{2\pi\bar{\varphi} M_1 Z_1^2 Z_2^2 e^4} \ln\frac{W_{\max}}{E_{\text{disp}}} \qquad W_{\max} = \frac{4M_1 M_2 E}{(M_1 + M_2)^2}, \tag{1.45}$$

where $W_{\max}$ is a maximum energy which is transferred in such a collision, M_1 is a mass of bombarding ions, M_2 is a mass of atoms in the target, E is the beam energy, E_{disp} is the displacement energy of target's atoms, Z_1 is a charge number of bombarding ions, Z_2 is a charge number of atoms in the target and $\bar{\varphi}$ is the beam flux [32].

The next part will describe the change in the scattering angles and changes in the beam emittance. When a charged particle passes through the material,the particle is deflected with many small-angle scatters by Coulomb scattering. This is shown on Figure 1.21. (However, for hadronic projectiles, the strong interactions also contribute to multiple scattering.). It is roughly Gaussian for small deflection angles, but at larger angles it behaves like Rutherford scattering, having larger tails than does a Gaussian distribution.

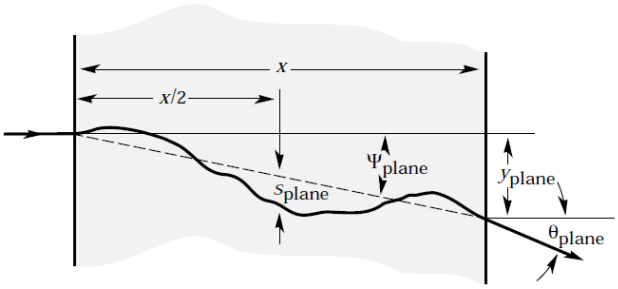

Figure 1.21: Multiple Coulomb scattering [33]

Referring to multiple scattering, that is the most common situation, naming θ the solid angle into which is concentrated the 98% of the beam after a thickness X of material, if we define $\theta_0 = \frac{\theta}{\sqrt{2}}$ as the projection of θ on a plane, the angular dispersion can be calculated by the following relation:

$$\theta_0 = \frac{13.6\,\text{MeV}}{\beta pc} Z \sqrt{\frac{X}{X_0}} (1 + \ln(\frac{X}{X_0})), \tag{1.46}$$

where β is a relativistic parameter, p is momentum c is speed of light, X is the foil thickness, X_0 is the radiation length of the material nad Z is a charge number of projectile.

The radiation length (X_0) is a characteristic of a material, related to the energy loss of high energy particles electromagnetically interacting with it and the characteristic amount of matter through which the particle has passed, usually measured in g/cm^2 . It is the mean distance over which a high-energy electron loses all but $1/e$ of this energy by bremsstrahlung. The radiation length for a given material of a single type of nucleus can be approximated by the following expression:

$$X_0 = \frac{716{,}4A}{Z(Z+1)\ln(\frac{287}{\sqrt{Z}})}, \tag{1.47}$$

where A is an atomic number of the target and Z is a charge number of atoms in the target.

The next consequence described is a change in the beam due to scattering. Angular distribution due to scattering that causes the beam spread and emittance growth has been described previously. The emittance of the beam before the stripping process is defined by the ion source and the aperture of the injector linac. After the stripping foil it changes and can be estimated by the following equation.

$$\varepsilon = \varepsilon_0 + \frac{\beta}{2}\theta^2_{\text{rms}}, \tag{1.48}$$

where ε_0 is the initial value of beam emittance, ε is the beam emittance after passing the stripping foil which caused beam sparing. Parameter β is the Twiss parameter. All processes mentioned above depend on the initial kinetic energy of the beam.

Charge exchange injection

It is possible to place the stripping foil into the injector linac before the entrance to the synchrotron or even in the synchrotron itself. By now we discussed the foil placed in the injector linac, but to achieve charge exchange injection the stripping foil is placed into the synchrotron.

Charge exchange injection is now the preferred injection method for high intensity machines. This allows us to inject ions many times into one and the same area in the phase space thus increasing the intensity of the stored beam. The charge exchange is generally accomplished by means of a stripping foil, which is also traversed by circulating particles. During injection it is important to minimize the number of foil hits per ion, since this leads to foil heating, emittance growth and beam losses.

1.8. Application of ions in radiotherapy

Today radiotherapy has an important part in the treatment of cancer. After surgery, radiotherapy is the most frequent and most successful form of therapy and more than 50% of patients with localized malignant tumors are treated with radiation. The biggest aim of radiotherapy is to deliver the dose in a perfectly precise way covering the tumor region, which means that the tumor receives 100% of the planned dose while the surrounding healthy tissues don't receive any dose [34].

In radiotherapy, in addition to the X-ray treatment, protons or light nuclei can be used. So a treatment beam can be made in the machine from protons, alpha particles, carbon ions, oxygen ions and etc.

In comparation between conventional radiotherapy and hadron therapy we can distinguish advantages of hadron therapy. These two advantages are a precise dose delivered with a finite range and a maximum dose deposition at the end of the range and a improved biological efficiency in the Bragg peak region. Using hadrontherapy with these advantages, we can deliver a large dose inside a deep tumor while the surrounding healthy tissue stays spared [35].

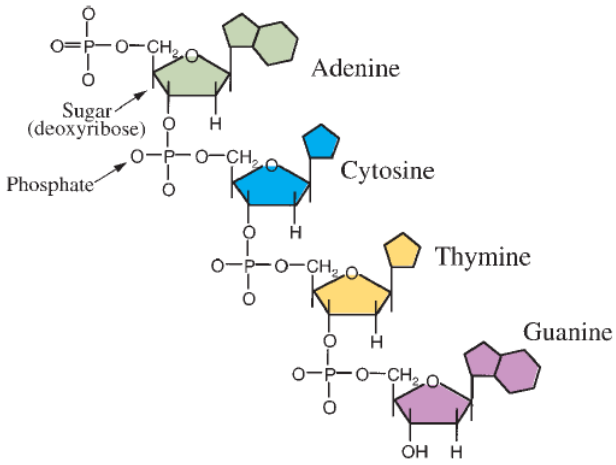

Figure 1.22: The structure of a single strand of DNA

Carbon ions and other heavier ions which have an atomic number Z higher then 6 ($Z \geq 6$) have one more advantage. They have increased biological efficiency which means that roughly one third of the dose from X-ray is needed if carbon ions are used. For protons and alpha particles this ratio is a bit lower, 10% for protons and 20% for alpha particles lower than the dose delivered by X-rays. Also, one more reason to use ions in cancer treatment is because they can destroy radioesistant and hypoxic tumors [34].

1.8.1. Damage on DNA and reparation

During interaction between tissues and radiation the main target is DNA. The biological effects of radiation are cell killing, carcinogenesis and mutation. These biological effects appear because of tracks of charged particles and the chemical changes. The DNA or the deoxyribonucleic acid is a large molecule with a double helical structure. It is composed of two strands which are linked by hydrogen bonds between the bases. The support to every strand consists of alternating sugar (this sugar is deoxyribose) and phosphate groups. The order of bases defines the genetic code. Two of the bases are single-ring groups or pyrimidines named thymine and cytosine. Two of them are double-ring groups or purines and they are named as adenine and guanine. The structure of a single strand of DNA is illustrated in Figure 1.22. The bases on opposite strands must be complementary, adenine pairs with thymine, and guanine pairs with cytosine. If the biological materials absorb any type of radiation (X-rays, gamma rays, charged and uncharged particles) then there exists a probability of interaction

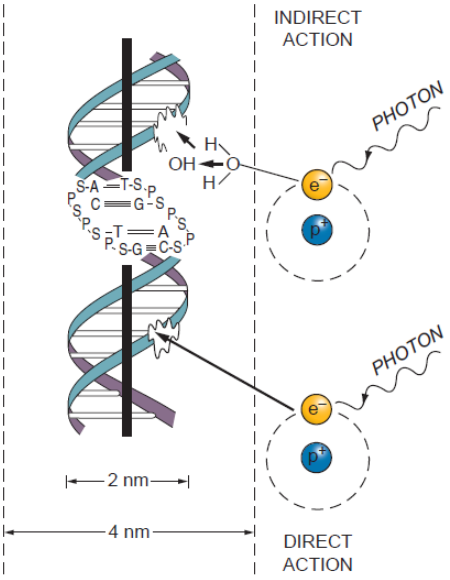

Figure 1.23: Direct and indirect actions of radiation

with DNA. The DNA's atoms will be ionized or excited which leads to a chain reaction which causes biological changes. These changes are called direct actions of radiation, this action is the dominant process if the radiation is composed with particles which have high linear energy transfer (LET), like alfa particles or neutrons. Also, radiation can interact with atoms or molecules producing free radicals that can go far enough to affect DNA. These types of interactions are reffered to as indirect action. Free radicals (like hydroxyl radical OH·) are atoms or molecules which have an unpaired electron in the outer shell. This state has a high degree of chemical reactivity. In direct action, secondary electrons are a consequence of absorbing photons from X-ray by DNA. In indirect interaction secondary electrons react with water molecules which produce OH groups. This OH molecule is a free radical that affects DNA. DNA has a diameter of 2 nm, but the estimation is that free radicals can produce damage on the DNA in a cylinder around the DNA with a diameter which is double so the diameter of the cylinder is 4 nm. Direct and indirect affect on DNA is shown on Figure 1.23.

On Figure 1.24 the first part which is labeled with A shows a simplified model of DNA. The radiation produces damage on DNA but DNA can fix some kinds of damage with reparation mechanisms. A dose of radiation that induces on average one lethal event per mammalian cell for X-rays is between 1 Gy and 2 Gy.

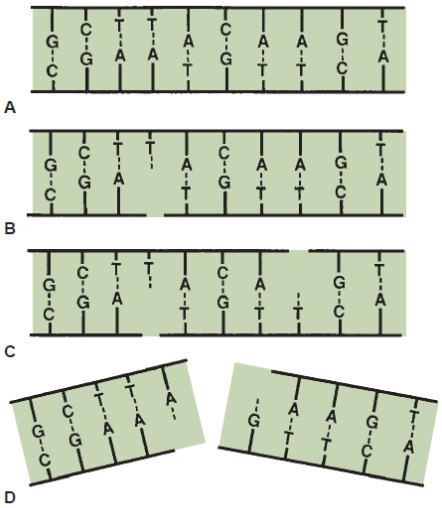

Figure 1.24: Diagrams of single- and double-strand DNA breaks caused by radiation

The number of DNA breaks per cell detected immediately after such a dose is approximately:

Base damage,>1,000
Single-strand breaks (SSBs), around 1,000
Double-strand breaks (DSBs), around 40

When the cells are irradiated with a certain dose of X-rays, DNA's single breaks or SSB- Single-strand breaks chain will appear. These breaks cannot cause cell death because cells have reparation processes and with these processes cells can fix these breaks. During the reparation of single strand brakes it is possible to create mutations and errors. Radiation which is powerful enough to produce double-strand breaks (DSBs) are ions such as carbon ions, oxygen ions ect. or protons. The probability of causing mutations and errors is much lower because double strand breaks cause cellular death [36].

1.8.2. Radiation-induced chromosome aberration

After interaction of ionizing radiation with the DNA it is possible for breaks to appear. A reparation process in the cells tries to fix the caused damage on the DNA but in some cases there is a probability of errors and faulty corrections. The chromosomes are built from DNA, so if the DNA is affected the logical

conclusion is that the chromosomes are affected also. There are many methods to measure the damage on the chromosome set.

Once breaks are produced, different fragments may behave in various ways:

- The breaks may restitute with and rejoin in their original configuration. In this case nothing amiss is visible at the next mitosis.
- The breaks may fail to rejoin and give rise to an aberration, which is scored as a deletion at the next mitosis.
- Broken ends may be reasserted and rejoin other broken ends to give rise to chromosomes that appear to be grossly distorted if viewed at the following mitosis.

For one organism which must go through radiation it is better to irradiate with hadrons because cells after this type of radiation will die with very high probability. This will prevent secondary cancer or some other disease in a new generation of descendants because there are no cells with mutations which will continue living mutated.

The aberration which can be seen at metaphase can be divided into two groups: chromosome aberrations and chromatid aberrations. If a cell is irradiated early in interphase, before the duplication of the chromosomes, then the damage will include single strand brakes of chromatin. When DNA is in the duplication process damages on the strand will be duplicated because an identical strand will appear. This way the damage was transferred to the next generation of cells and this is the method by which **chromosome aberrations** are produced. On the other hand if a cell is irradiated later in interphase, after the DNA material has doubled and the chromosomes contain two strands of chromatin, that will lead to **chromatid aberrations**. Some of aberrations are shown on Figure 1.25 [36].

1.8.3. Relative biologic effectiveness (RBE)

The dose which is produced by 250 kVp of X-rays makes certain biologic effects in the tissue and this is considered referent radiation. Relative biologic effectiveness is the ratio of doses from 250 kVp of X-rays and some other radiation which makes the same biological effect in the tissue.

$$RBE = \frac{D_{250}}{D_r}, \tag{1.49}$$

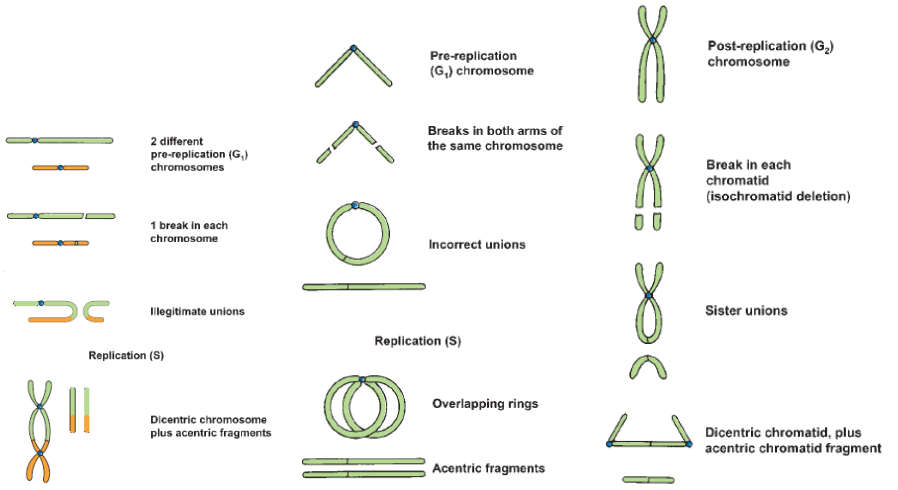

(a) The steps in the formation of a dicentric.

(b) The steps in the formation of a ring.

(c) The steps in the formation of an anaphase bridge.

Figure 1.25: Example of chromosome aberrations

whereD_{250} and D_r are, respectively, the doses of X-rays and the test radiation required for equal biologic effect.

The example is that 1 Gy of carbon ions produce a greater biologic effect than 1 Gy of X-rays. This biologic effect means that the radiation kills cells, creates tissue damage, mutations etc. Sometimes the gamma radiation from Cobalt 60 (1.25 MeV) or the megavoltage X-ray is chosen as the referent radiation.

Radiation biologic effectiveness (RBE) is directly related to LET (linear energy transfer). This means that high RBE implies high LET. As it is mentioned earlier charged particles have high LET so the radiation with ions has high RBE. Since, the LET of a charged particle is increasing as the particle is slowing down (because of the Bragg peak) then RBE is increasing too as the particle is slowing down [20].

Historically scientists through experiments have been investigating the effects of radiation on living cells and biological systems. In almost every study the cell's survival was measured as a function of the absorbed dose. The cell's death was defined as complete loss of the proliferation capacity. The obtained curves show characteristic slopes which can be interpreted as the biological effectiveness of the applied radiation. The curves of survival fraction have non-linear behavior and survival S is plotted in log-scale unlike dose D which is linear scale. Radiosensitivity is small at low doses because most of the damage can be repaired, but at higher doses the sensitivity increases and the slope of the curves decreases

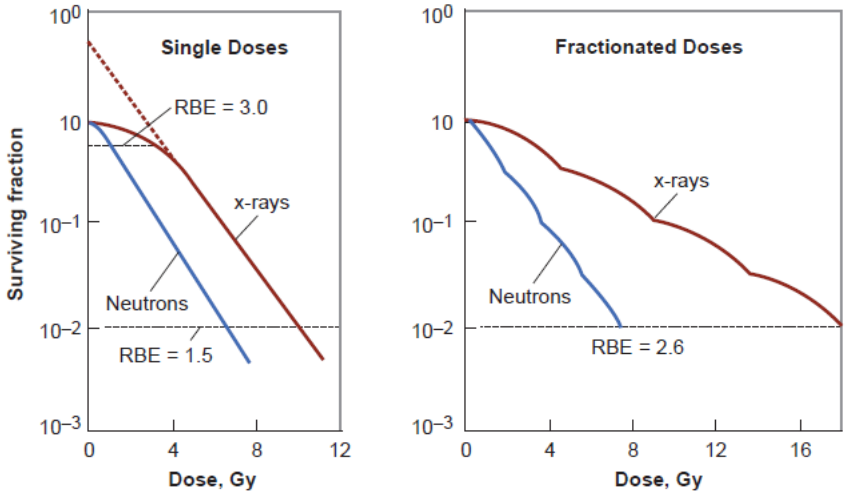

(a) Single doses (b) Fractionated doses

Figure 1.26: Typical survival curves for mammalian cells exposed to X-rays and fast neutrons

more and more. This can be expressed with a linear-quadratic equation:

$$S = \exp(-\alpha D + \beta D^2), \tag{1.50}$$

where S is a survival fraction, the coefficient α is the slope at small doses and from α it is possible to get the initially produced irreparable damage. The parameter β shows reparable effect at higher doses. The ratio of two of these parameters α/β is a measure for the repair capacity of the cells. The typical values are from 1 Gy to 3 Gy for cells with high repair capacity and near 10 Gy for the cells which don't have repair potential [34]. The graphs on Figure 1.26a are survival curves obtained when mammalian cells in cultures are exposed with a range of doses. Two types of radiation neutrons and 250 kVp X-rays were used in the experiment. Now the RBE will be calculated by the Equation (1.50) which is mentioned earlier. On the y-axis the surviving fraction is represented and on x-axis the doses are represented. A couple of values of the survival fractions and corresponding RBE are considered. First is a surviving fraction of 0.01. For 0.01 the RBE is 1.5, the next value is a surviving fraction of 0.6 and for this fraction the RBE is 3.0. Generally the RBE increases as the dose decreases. Higher RBE can be obtained if fractionated radiation is used which isn't accomplished by single exposure. This is because in fractionated radiation small doses are used which imply higher RBE. On Figure 1.26b a hypothetical radiation treatment with 4 fractions is shown and for the survival fraction of

0.01 the RBE of neutrons radiation is 2.6 unlike the X-rays, which is proof to the fact that the RBE is higher in the fractionated treatment with small doses [36].

1.8.4. Radioresistant tumors and tumor's hypoxia

Ionizing radiation is one of the most effective ways to treat cancer, however because of the radioresistance of certain tumors conventional radiotherapy options are often limited. During the radioresistance process the tumor cells or tissues adapt to the radiotherapy. It is known that the presence or absence of molecular oxygen has an effect on the biological aspect of ionizing radiation and this is a condition for radioresistance development. This condition is called the hypoxic condition. It is proven that the lack of oxygen results in inefficient formation of DNA strand breaks with ionizing radiation and prevents the repair mechanisms. The development of radioresistance leads to a poor prognosis for the patient and it is the main reason for radiotherapy failure, which leads to tumor recurrence, regrowth and metastases. Among the methods suggested to overcome this problem are treatments in hyperbaric oxygen chambers and the introduction of high linear energy transfer (LET) radiations, such as protons and heavy ions [36–38].

1.8.5. The depth dose distribution and variations

The dose distribution per depth or absorbed dose in the patients is formed when the incident beam enters the patient. The dose distribution is affected by many factors such as beam energy, the type of particles in the beam, depth, field size, distance from source, beam collimation system, the type of tissue and so on. So, when someone prepares a treatment plan, these factors must be considered and taken into account.

One of the most important steps in dose calculation is to define the dose variation in tissue along the central axis of the beam. The dose distribution has expressed over percentage of the initial dose and this can be measured by some dosimetry systems such as ionization chambers, thermoluminescent dosimeters (TLD), diodes, and film are occasionally used. But, in practice the preferred method is to use ion chambers because they have better precision and smaller energy dependence.

The way of characterizing the central axis is to normalize the dose at a depth with regards to the dose at reference depth. So, the easier way to express this

distribution is to calculate the percentage depth dose which is a percentage of the absorbed dose at any depth d to the absorbed dose at a reference depth d_0 along the central axis of the beam. Percentage depth dose (PDD) is then

$$PDD = \frac{D_{\mathrm{d}}}{D_{\mathrm{d_0}}} \times 100\%, \tag{1.51}$$

where D_d is a dose on depth d, and D_{d_0} is a dose on a reference depth d_0.

The reference depth may also vary from case to case but the deal is that for orthovoltage (up to about 400 kVp) and lower-energy X-rays the reference depth is on the surface ($d_0 = 0$). For higher energies the reference depth is at the position of the peak absorbed dose ($d_0 = d_{\mathrm{m}}$) which also depends on the beam energy. The peak absorbed dose has several names and sometimes it is called the maximum dose, the dose maximum, the given dose or just simply the D_{max}.

$$D_{\mathrm{max}} = \frac{D_{\mathrm{d}}}{P} \times 100\%. \tag{1.52}$$

The depth dose decreases with depth beyond the depth of maximum dose and increases with beam energy. High energy beams have grater penetrating power and deliver the dose very precisely or if carbon ions are used they deliver the dose with very high precision due to the Bragg peak.

As it is mentioned earlier the depth dose distribution is influenced by many factors, but the most important are the type of particles in the beam and the beams energy. Today, in the world different particles are used in tumor therapy. The most efficient are carbon ions but their use in practice is very hard because of large financial costs. Carbon ions are used in just 13 oncological centers in the world. X-ray machines have good precision, but they don't have Bragg peak

X-ray radiation is the most common method for cancer treatment in the world. However, the fact is that differences exist in the efficiency and dose distribution in a patient. The aim of radiotherapy is that the dose which is calculated during the development of a radiotherapy treatment plan is delivered on the most accurate possible way in the tumor. During this procedure it is mandatory to save and preserve the patient's skin, sensitive tissues and his organs. The best way to protect all tissues, through which radiation passes before reaching the tumor, is by using carbon ions and protons because of the Bragg peak. However, these techniques with protons and carbon ions are hardly available instead of them other techniques which use X-rays have been developed. Some of them are Image-Guided Radiation Therapy (IGRT), Intensity-Modulated Radiation Therapy (IMRT) or Three-Dimensional Conformal Radiation Therapy (3D conformal) radiotherapy. These techniques have made great progress in con-

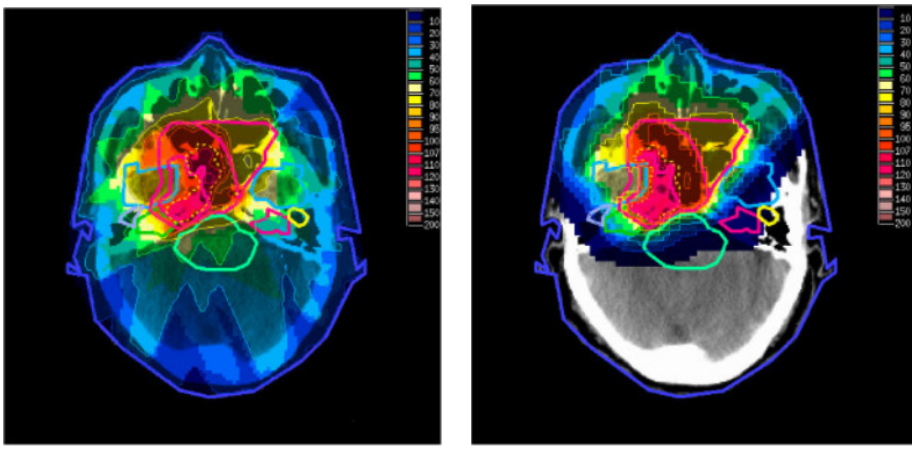

(a) Depth dose distribution for X-rays. (b) Depth dose distribution for protons.

Figure 1.27: The differences in dose distribution between X rays and protons[39].

ventional radiotherapy. The interesting fact is that today scientists are testing oxygen ions for use in radiotherapy and they express very good performances in destroying radioresistant tumors. It should be noted that on images, but in general radiotherapy treatment developing as well, hot regions or high dose regions are indicated with red color and cold regions or low dose regions are indicated with blue color [36].

On Figure 1.27 and Figure 1.28 a depth dose distribution is shown for X-rays, protons and carbon ions. The differences in the distribution are very evident and it's visible that protons and carbon ions protect the tissue which surrounds the tumor and this is very important in preventing organ damage or the development of a secondary tumor. Another advantage of protons and carbon ions unlike X-rays is that during fractionation radiation the dose which the patient receives with X-ray radiation, the same dose can be delivered with carbon ions or protons during a significant lower number of fractions. The next important thing to note is that with carbon ions the treatment is performed with a lower number of input filed on the patient's skin [20, 41].

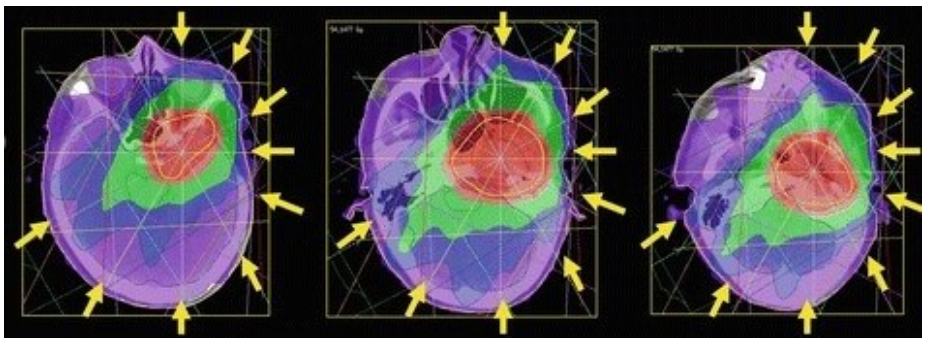

(a) Depth dose distribution for X-rays.

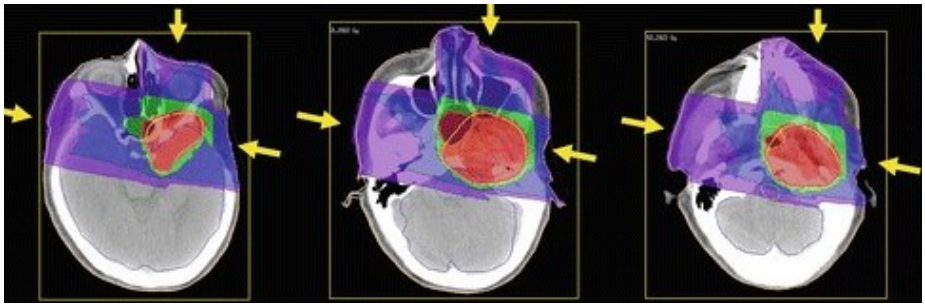

(b) Depth dose distribution for carbon ions.

Figure 1.28: The differences in dose distribution between X-rays and carbon ions for three slices [40]

Chapter 2

Materials and Methods

2.1. LISE ++

The program LISE++ is designed to predict the intensity and purity of radioactive ion beams (RIB) produced by magnetic separators. LISE++ also facilitates the tuning of experiments where its results can be quickly compared to online data. The program is constantly expanding and evolving from the feedback of its users around the world.The aim of LISE++ is to simulate the production of RIBs via some type of nuclear reactions (projectile fragmentation, fusion-residual, fusion-fission, coulomb fission, and abrasion-fission.) (Several are available in the program), between a beam of stable isotopes and a target.

The program simulates the characteristics of the nuclear reactions based on well-established models, as well as the effects of the altering device located downstream of the target used to create the RIBs.

2.2. ETACHA 4

ETACHA 4 is a program for calculating charge states at GANIL energies.The Grand Accélérateur National d'Ions Lourds (GANIL), or Large Heavy Ion National Accelerator, is a French national nuclear physics research center in Caen. The facility has been in operation since 1983, and consists primarily of two serialised synchrocyclotrons. A computer program calculating charge state distributions of ions with up to 28 electrons distributed over n = 1, 2 and 3 subshells has been developed. The model is based on an independent electron model

taking into account electron loss, capture and excitation from and to all the subshells. Calculated atomic cross sections are recomputed periodically to take into account their dependence with the projectile energy and its mean charge state when they vary as a function of target thickness.

2.3. MATLAB

MATLAB (matrix laboratory) is a multi-paradigm numerical computing environment and proprietary programming language developed by MathWorks. MATLAB allows matrix manipulations, plotting of functions and data, implementation of algorithms, creation of user interfaces, and interfacing with programs written in other languages, including C, C++, Java, Fortran and Python. MATLAB is used by engineers and scientists in many fields such as image and signal processing, communications, control systems for industry, smart grid design, robotics as well as computational finance.

2.4. SRIM

Stopping and Range of Ions in Matter (SRIM) is a group of computer programs which calculate interaction of ions with matter; the core of SRIM is a program Transport of ions in matter (TRIM). SRIM is popular in the ion implantation research and technology community and also used widely in other branches of radiation material science. Also, this program allows us to calculate the damage of a target. These calculations are based on the Monte Carlo simulation. The Monte Carlo simulation is used to model the probability of different outcomes in a process that cannot easily be predicted due to the intervention of random variables. It is a technique used to understand the impact of risk and uncertainty in prediction and forecasting models. The Monte Carlo method can be used to tackle a range of problems in virtually every field such as finance, engineering, supply chain, and science. This simulation is also referred to as multiple probability simulation.

2.5. Gnuplot

Gnuplot is a command-line program. It can generate 2D and 3D plots of functions, data, and data fits. Gnuplot is a program dating from 1986.

Gnuplot can produce output directly on screen, or in many formats of graphics files, including Portable Network Graphics (PNG), Encapsulated PostScript (EPS), Scalable Vector Graphics (SVG), Joint Photographic Experts Group (JPEG), and many others. It is also capable of producing LaTeX code that can be included directly in LaTeX documents, making use of LaTeX's fonts and powerful formula notation abilities. The program can be used both interactively and in batch mode.

It can read data in multiple formats, create multiple plots on one image, do 2D, 3D, contour plots, parametric equations, supports various linear and non-linear coordinate systems, projections, geographic and time data reading and presentation, box plots of various forms, histograms, labels, and other custom elements on the plot, including shapes, text and images, that can be set manually, computed by script or automatically from input data. The gnuplot is programmed in C programming language.

Chapter 3

Results and Discussion

3.1. Stripping efficiency

The carbon foil stripping efficiency was estimated using a LISE ++ program which simulates the stripping process. The results are shown in the following graphs.

The aim of estimating the stripping efficiency of the foil is to determine the best location of the stripping foil along the accelerator.

The estimating is done for different thicknesses of foil: 1.77 µm, 0.88 µm, 0.44 µm, 0.75 µm and 0.08 µm. The foil with 0.08 µm doesn't exist because it is imposible to produce a foil with that thickness, it is too thin. Also, the estimation was done with different projectiles. Carbon ions, argon ions, oxygen ions, and neon ions are chosen for the projectiles. The initial ions charge was selected with the charge to mass ratio (q/m) which has to be larger or equal to 1/3, because the future linac will be design for this mass-to-charge ratio. Larger mass-to-charge ratio particles can still be accelerated by lowering the amplitude of the accelerating field, but lower mass-to-charge ratio particles would require higher accelerating fields well outside of the design fields. Following this ratio, the initial charged states are C^{4+}, C^{5+}, Ar^{12+}, O^{6+} and Ne^{6+}. The foil stripping efficiency depends on the initial beam kinetic energy and foil thickness. The realistic energies in the injector linac are between 0.4 MeV/u and 10 MeV/u, where lower limit is determined by the beam energy after a short RFQ while the 10 MeV/u is the largest energy investigated for the new synchrotron.

In the frame of LISE++ software it is possible to select two different integrations types ordinary differential equation solver (ODE) and Runge-Kutta-Fehlberg solver (RKF), and the differences between these two integrations types are compared.

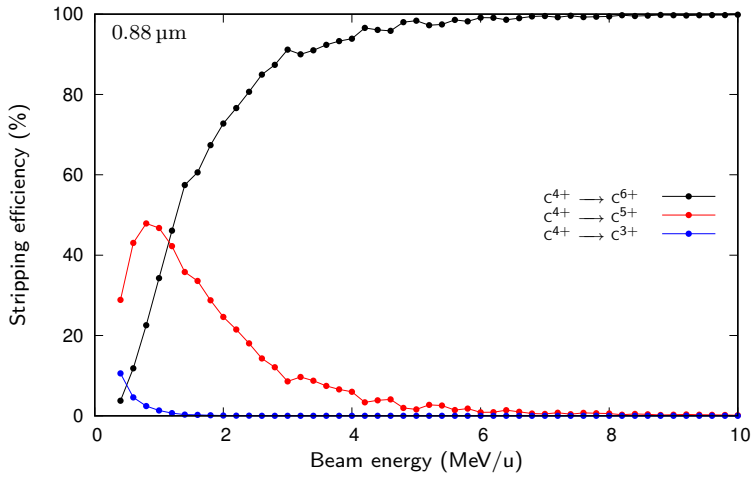

Figure 3.1: Stripping efficiency for C^{4+} carbon ions

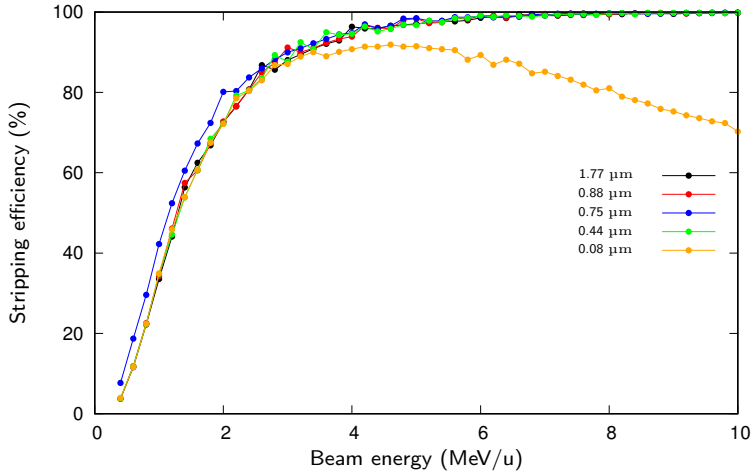

Figure 3.2: Stripping efficiency for different thicknesses of carbon stripping foil

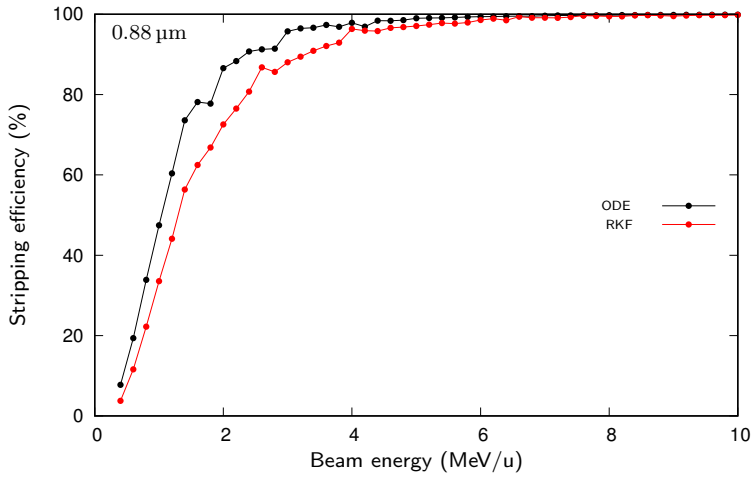

Figure 3.3: Differences in result precision between two integration methods

In case when for stripping efficiency estimating we use C^{4+} ions the results are shown on Figure 3.1. For the foil thickness of 0.88 µm and for the initial kinetic energy from 3 MeV/u to 4 MeV/u the stripping efficiency for C^{4+} in C^{6+} is around 90%, for kinetic energy above 6 MeV/u, the presence of C^{6+} is almost 99%. On graph are shown percentages of getting C^{5+} but after 2 MeV/u the curve falls down on zero, while the probability that ion accepts the electron is negligible.

On Figure 3.2 the stripping efficiency for the different carbon foil's thicknesses is shown. It can be noted that with the increase of energy above 5 MeV/u at very thin films (0.08 µm) the efficiency is lost. The foils with thicknesses 0.88 µm and 0.75 µm have the best results in stripping efficiency where is 200 $\frac{\text{mg}}{\text{cm}^2}$ and 300 $\frac{\text{mg}}{\text{cm}^2}$ of surface thicknesses, respectively.

The graph on Figure 3.3 shows differences in the precision of the two integration methods ODE and RKF. The ODE method is less accurate and gives an unstable curve while the RKF is more accurate and the resulting curve is more stable. During the simulation run, it took more time to calculate the RKF integration method than ODE. The distance between curves gives us an idea about uncertaining of models.

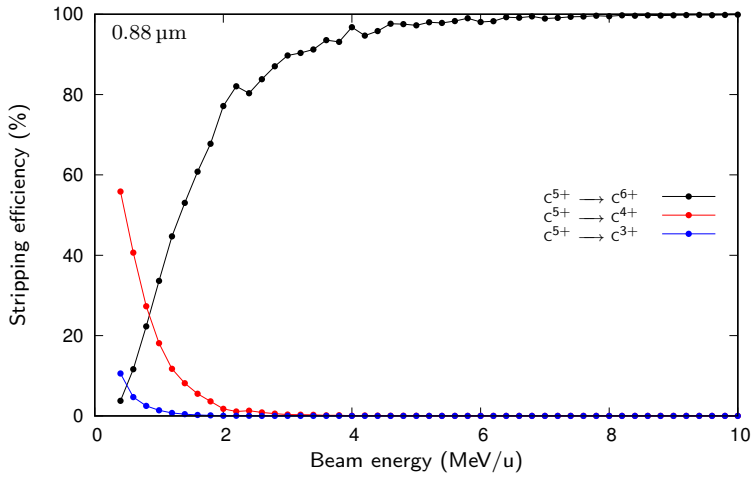

Figure 3.4: Stripping efficiency for C^{5+} carbon ions

Carbon foil stripping efficiency for the carbon ions from C^{5+} to C^{6+} is shown on Figure 3.4. The efficiency for getting C^{6+} from C^{5+} is 90% for the initial kinetic energy of 4 MeV/u. The foil thickness is 0.88 µm. The maximum efficiency is 99% for energies above 5 MeV/u. The presence of C^{4+} and C^{3+} has a very low probability for whole energies interval and after 1 MeV/u their presence is negligible.

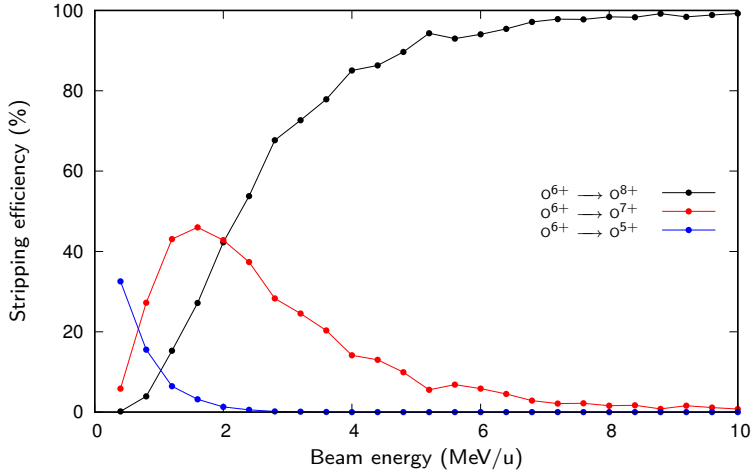

Figure 3.5: Stripping efficiency for O^{6+} oxygen ions

Carbon foil stripping efficiency for the oxygen ions from O^{6+} to O^{8+} is shown on Figure 3.5. The efficiency for getting O^{8+} from O^{6+} is 90% for the initial kinetic energy of 6 MeV/u. The foil thickness is 0.88 µm. The maximum efficiency is

99% for energies above 8 MeV/u. The presence of O^{7+} and O^{5+} has a very low probability for whole energies interval and after 5 MeV/u their presence is negligible.

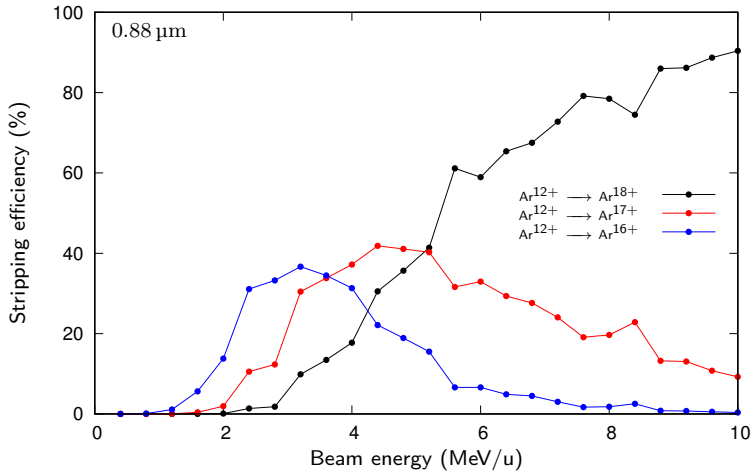

Figure 3.6: Stripping efficiency for Ar^{12+} argon ions

The carbon foil stripping efficiency in the argon ions case is shown on Figure 3.6. The results give very inefficient stripping probability and the curve looks unstable. The maximum efficiency is 85% for 10 MeV/u initial kinetic energy. The reason for inefficient stripping with carbon foil is that argon is a quite heavy ion and it's hard to break the bond between argon's nucleus and its electrons.

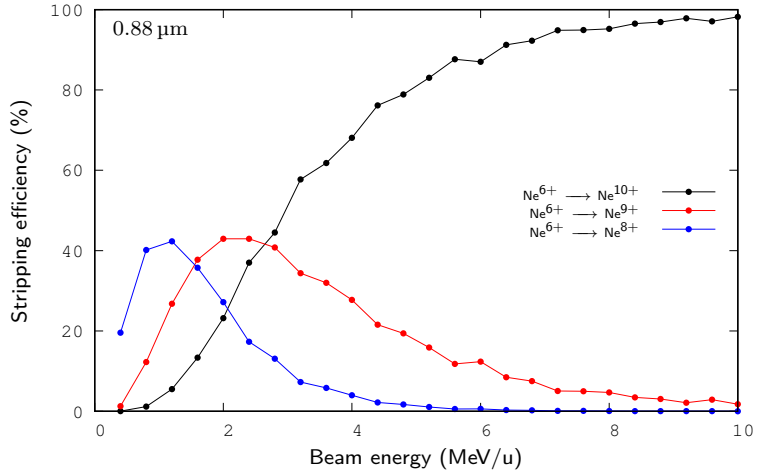

Figure 3.7: Stripping efficiency for Ne^{6+} neon ions

Figure 3.7 shows the efficiency of obtaining a neon nucleus, ie. obtaining Ne^{10+} from Ne^{6+}. For energy of 8 MeV/u the efficiency is about 90%, and for energy of 9 MeV/u and above the efficiency is about 99%. The foil thickness is 0.88 μm.

3.2. Emittance blow-up

As the beam passes through the foil, interactions between the beam and the foil material start to take place. The dominant interaction is multiple Coulomb scattering. The scattering angles are dependant on the particles' initial kinetic energy. Resulting data was obitained by MATLAB coding and the Equation (1.48) which are described in Chapter 1. In the Equation (1.48) the value of ε_0 was 0.75 mm mrad, the beta β optic function was 2 m. The scattering angles were obtained by Equation (1.46) , where β and p depend on the velocity of the ions whose values were obtained by the initial beam kinetic energy. The speed of light c is $3 \times 10^8 \frac{\mathrm{m}}{\mathrm{s}}$. X depends on the foil thickness in mg/cm^2, and X_0 is obtained by the Equation (1.47). The X_0 value for carbon foil is 43 $\frac{\mathrm{g}}{\mathrm{cm}^2}$.

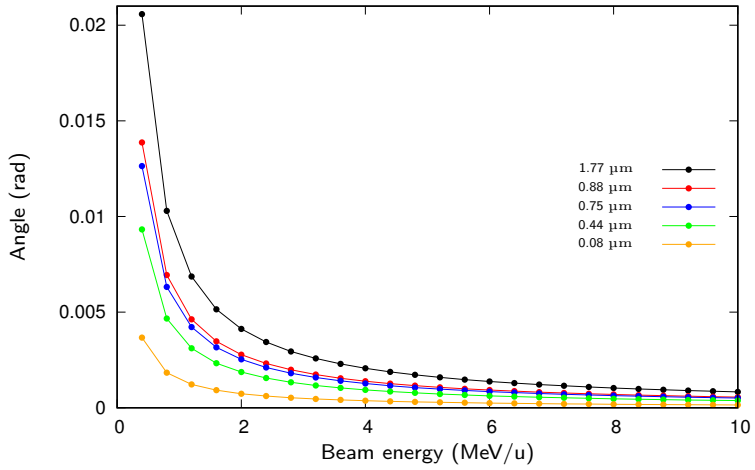

Figure 3.8: Scattering angles for C^{4+} carbon ions

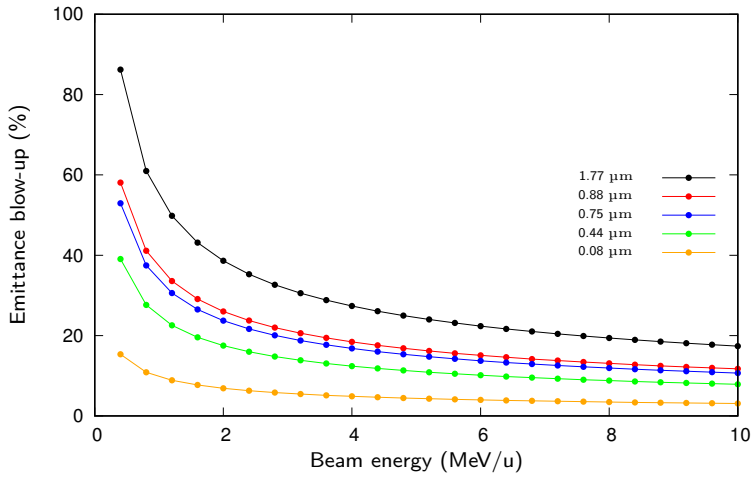

Figure 3.9: Emittance blow up for C^{4+} carbon ions

Figure 3.8 shows the relationship between the average scattering angle (because the beam consists of a number of particles of order 10^{10}) and the kinetic energy of the beam. It can be observed that with increasing energy these angles become smaller and with lower kinetic energy the value of angles becomes larger for all film thicknesses. With higher energy, the beam has a higher velocity, which determines the shorter time it takes the beam to pass through the foil, which results in a lower ampitude of interaction. On the other hand, the thicker the foil, the greater the amount of atoms and the grater likelyhood of interaction. The smallest average scattering angles give the thinnest film 0.08 µm, but this film does not have enough efficiency, while the thicker film 1.77 µm has the highest average scattering angles. All angle values are in the range of 0.1 mrad to 21 mrad. Average scattering angles of 10 MeV/u for different thicknesses of 1.77 µm, 0.88 µm, 0.44 µm, 0.75 µm and 0.08 µm are respectively 0.8 mrad, 0.55 mrad, 0.37 mrad, 0.5 mrad and 0.14 mrad.

Multiple scattering causes change in one important beam parameter in the accelerator. That parameter is beam emittance. As the scattering angles are larger than the beam emittance is larger. Figure 3.9 shows results for geometric emittance blow-up. On this graph, it can be noticed that with higher energy the changes from initial values are smaller. The beam emittance growth is directly dependent on the scattering angle and straightforward is that it has the same energy and foil thicknesses dependency as multiple scattering. The thinnest foil has the smallest emittance change and the thickest foil has the largest.

This results were obtained assuming that the stripping foil is in the injector linac, before entrance in synchrotron.

3.3. Temperature

When the beam passes through the stripping foil energy release starts to occur and the foil starts to heat up. The increase of the foil temperature is calculated with the Equation (1.44). To calculate the volume V a disc shaped foil with the radius of 3 mm was used. Different foil thicknesses 1.77 µm, 0.88 µm, 0.44 µm and 0.75 µm had the respective volumes $50.02 \times 10^{-3}\,\mathrm{mm}^3$, $24.87 \times 10^{-3}\,\mathrm{mm}^3$, $21.2 \times 10^{-3}\,\mathrm{mm}^3$ and $12.43 \times 10^{-3}\,\mathrm{mm}^3$. Specific heat capacity c_p for the carbon foil is 0.71 J/gK . $\mathrm{d}E/\mathrm{d}x$ stopping power of the carbon ions in the carbon foils was obtained using the ETACHA 4 program. The density of the carbon foil is 2.55 $\frac{\mathrm{g}}{\mathrm{cm}^3}$, while the number of carbon ions assumed in the calculation was 2×10^{10} The calculation was performed for C^{4+} ions.

The results are obitained by MATLAB and shown on Figure 3.10.

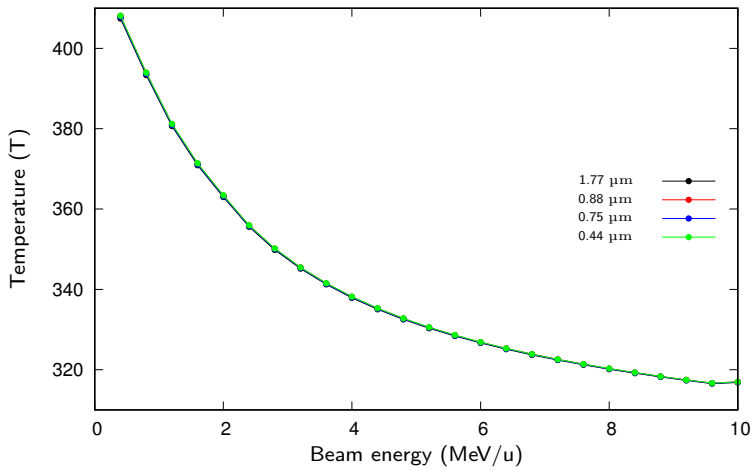

Figure 3.10: Foil's temperature for C^{4+} carbon ions

The represented temperatures are the final temperatures, which means that they are the temperature increases (ΔT) plus the initial room temperature which is 293 K. It can be seen that all temperature values did not dependent on foil thickness, they are only dependent on initial beam kinetic energy. All obitained final temperatures for all energies are under the melting point of the carbon stripping foil. The melting point for the carbon stripping foil is 3500 K. It should be emphasized that the equation which is used does not take into account heat dissipation.

3.4. Radiation damage

These graphs were obtained using SRIM, a program which is used to simulate the target damage, in this case the target is the carbon foil. The simulation was carried out on 3000 ions for a 1 µm foil. On the left side are graphs for 7 MeV/u ion energies and on the right for 10 MeV/u energies. The reason why these two energies where chosen is to show the extent of the damage on the foils which are used today as the energy of the beams used today are 7 MeV/u in comparison to the 10 MeV/u energies that are to be used in new facility in the future.

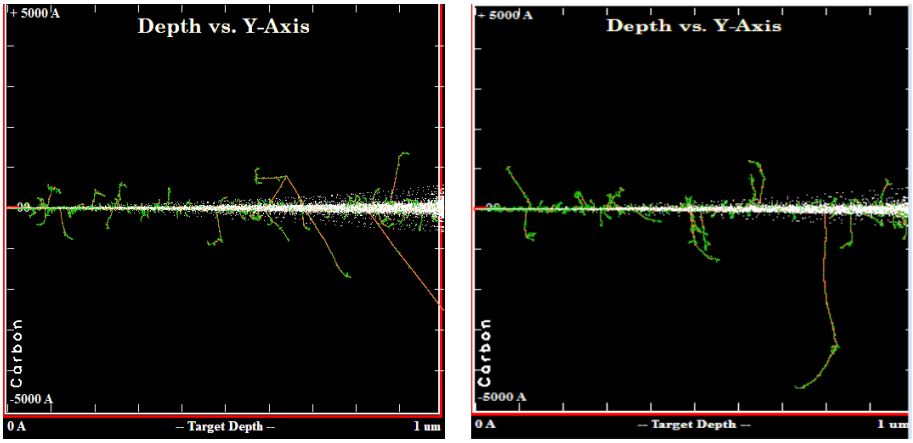

(a) Energy 7 MeV/u (b) Energy 10 MeV/u

Figure 3.11: Simulation of C^{4+} beam passes throught the stripping foil

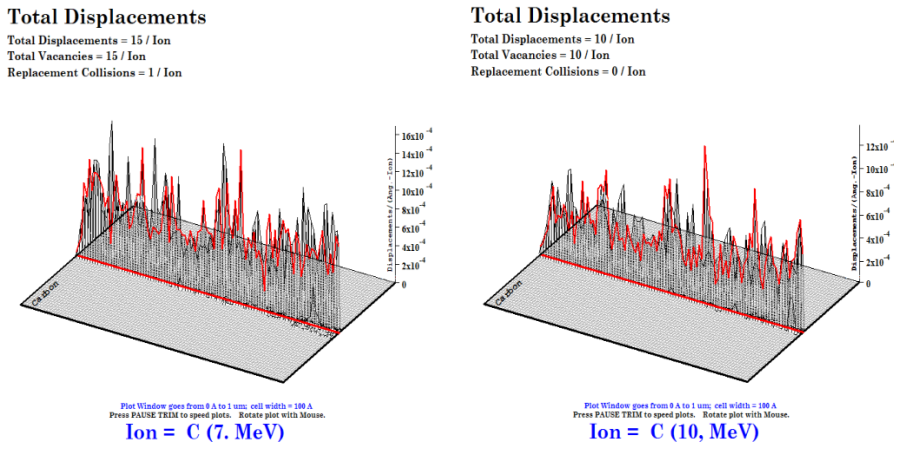

(a) Energy 7 MeV/u (b) Energy 10 MeV/u

Figure 3.12: Total displacement along carbon stripping foil

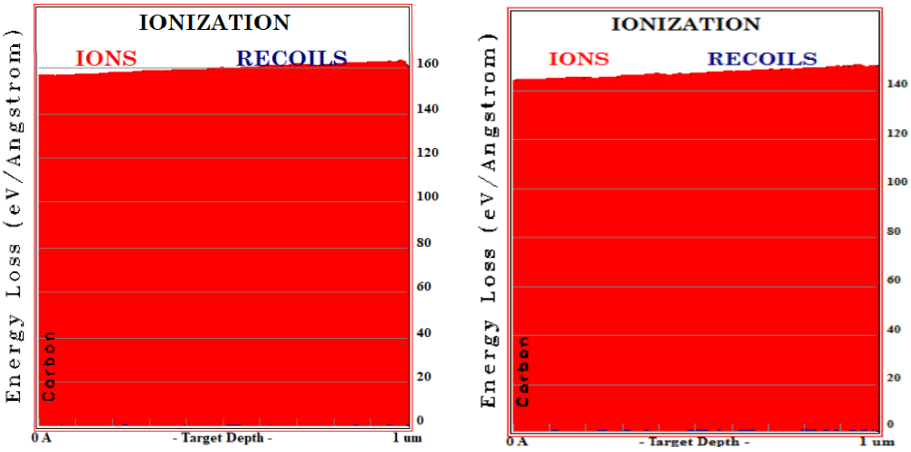

(a) Energy 7 MeV/u (b) Energy 10 MeV/u

Figure 3.13: Energy transfer along carbon stripping foil

Figure 3.11 shows us the trajectory of the ions through the foil. The red dots are collisions between the ion and target atoms in which the target atoms are knocked from their lattice sites. The green dots are collisions between recoiling target atoms and other target atoms. The recoiling target atoms cause collision cascades which dominate the damage process. The dot is only plotted if the transferred energy is large enough to displace the atom hit from its lattice site.

From Figure 3.12 can be noticed that there is a smaller number of movements is made by the beam with the higher energy which was proven earlier and also that higher energy beams cause less damage. It can be seen from the graph that the total displacement for a beam with the energy 7 MeV/u that there are 15 movements per ion and for a beam with the energy of 10 MeV/u there are 10 movements per ion. The same values are related to the number of vacancies, for the replacement collisions we have 1/ion for a beam of 7 Mev/u and 0/ion for 10 MeV/u.

Another marker of foil damage is the dsiplacement per atom (dpa) which is calculated by the following equation:

$$dpa = \frac{n_d}{density\ of\ target} \cdot \phi, \tag{3.1}$$

where n_d is the number of displacements in dimension of $displeacement/cm$, $density\ of\ target$ is in dimension of $atoms/cm^3$ and ϕ is integrated flux beam particles in the beam center in dimension of $1/cm^2$.

For a number of ions of 2×10^{10} dpa for case of 7 MeV/u is 1.61×10^{-8} , and for 10 MeV/u is 1.23×10^{-8} which tells us that the extent of the damage is very small. For the yearly operation the dpa in case of 7 MeV/u is 3.87 and for 10 MeV/u is 6.25 , but during calculation it is considered that machine working whole year 24 hours per day which is not reality, this numbers are smaller.

Figure 3.13 displays energy lost to the target electrons (Equation (1.41)). The electrons of the target absorb energy from the fast moving ions and recoil atoms The plot shows ionization from the incident ions and also from recoiling target atoms. From these graphs we see that in this case the energy which is lost by the travel length is lost to the transfer of energy from the ions onto the electrons in the foil. For a beam with the energy of 7 MeV/u the energy loss per travel length from the beginning to the end of the foil is from 150 eV/angstrom to 160 eV/angstrom. For a beam with an energy of 10 MeV/u this value is from 140 eV/angstrom to 150 eV/angstrom. The conclusion is that a higher energy beam looses less energy per unit of travel which means that less energy is transferred onto the foil atoms and hence the foil damage is smaller than with a beam with a starting energy of 7 MeV/u.

The foil lifetime is calculated by the Equation (1.45) which has the following parameters: $E_{\text{disp}} = 34$ eV, M_1 and M_2 have the values of 12, $Z_1 = 4$, $Z_2 = 6$, fluxes for 7 MeV/u and 10 MeV/u are respectively $\bar{\varphi} = 1.9 \times 10^{14}\, 1/\text{cm}^2\text{s}$ and $\bar{\varphi} = 2.2 \times 10^{14}\, 1/\text{cm}^2\text{s}$, elementary charge $e = 1.6 \times 10^{-19}$ C, and E is the beam energy in joules. The results which were obtained show that the foil will last longer and have a longer lifetime If a 10 MeV/u beam is used, where the lifetime is calculated to be 58.5×10^8 s, in contrast to 47.3×10^8 s when 7 MeV/u beam is used.

There is a distinct difference in the values obtained with the SRIM simulation (over dpa) in comparison to the values obtained by using Equation (1.45). It can be concluded that the SRIM simulation underestimates the lifetime of the stripping foils.

In a private discussion with key personel from dkfz clinic in Heidelberg, I have received information that the stripping foils are replaced once a year and that they have also confirmed a very long lifetime of the foil.

3.5. Charge-exchange injection

Charge exchange injection was simulated by MATLAB tools. The MATLAB script which is used for calculation is based on loop over injection time.

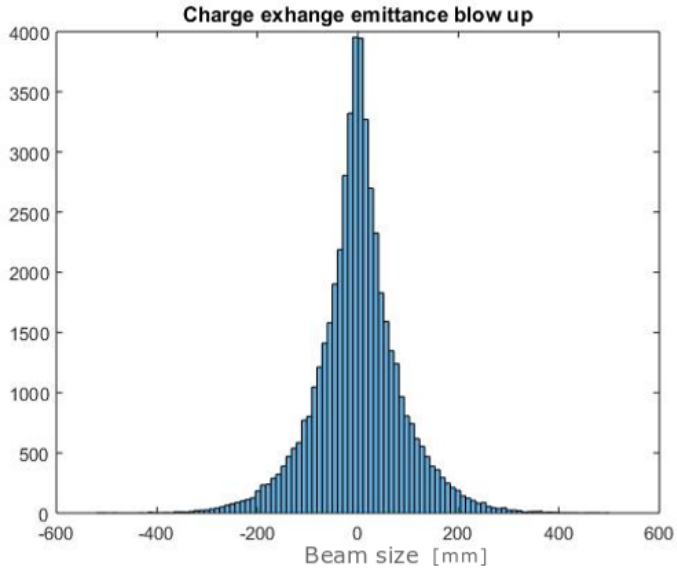

Figure 3.14: Non gaussian distribution of the particles in the beam

The time step (Δt) was 2 μs and the injection time interval was 64 μs. In this case for the beam which has 2×10^{10} ions an incerase in the temperature, for one injection trough the carbon foil, is around 350 K. The final foil temperature, when we add 293 K the room temperature, is around 650 K. The assumption was that the beam had a Gaussian distribution but the simulation for a beam emittance blow up lead to conclusion that beam is not Gaussian anymore. The Figure 3.14 with the histogram, shows this non gaussian distribution. The exepted sigma for gaussian distribution is 72.0788 mm and the obtained standard deviation is 85.3524 mm which is 18% larger in respect to initial. The estimated foil lifetime is 36×10^7 s.

Based on the results obtained, it can be concluded that the foil damage is in acceptable quantities. The lifetime of the foil is long, the temperature increase of the film is below the carbon melting point but slightly higher than the foil placed in the linac. An important change that has occurred is that the distribution of particles before and after the foil is not the same, ie. the Gaussian distribution is lost after the particles pass through the foil.

Chapter 4

Conclusion

The main aim of this research is to investigate the optimum location of stripping foil in carbon therapy facility. It is a part of broader study on possibility injection of 2×10^{10} C^{6+} into a medical synchrotron. Typically used ECR ion sources produce much more C^{4+} ions than C^{6+}. A stripping foil allows for reaching maximum charged state. The stripping process efficiency depends on beam energy and, at the same time, acceleration is more efficient for higher charged states (makes linac shorter). Therefore, an optimal location for the stripping foil, estimating its temperature, impact on the beam divergence and lifetime due to radiation damage is determined. The stripping efficiency is also estimated for other kind of ions, relevant for medical facility: C^{4+}, C^{5+}, Ar^{12+}, O^{6+} and Ne^{6+}.

The results of the simulations, calculations and the data analysis have shown that carbon based stripping foils are very efficient and durable. The stripping process may be considered efficient after 4 MeV/u energies for all relevant ions for medical purposes. The results have also shown that the foil is more durable and is less damaged if higher energy beams are passed through it hence by increasing the beam energy the foil is less exposed to damage. From the graphs it can also be seen that the angles of scattering are smaller in this case. This results in less scattering which leads to smaller emittance. The increase of emittance for a foil thickness of 0.2 $\frac{\text{mg}}{\text{cm}^2}$ in relation to the starting value is 14% for energy of 7 MeV/u which is the same as the values from PIMMS, and for a value of 10 MeV/u the increase of emittance is 12%. Also the foil heating in that case is reduced and doesn't depend on the foil thickness for foils this thin. All calculated temperatures are below the melting point of the carbon foil which

is 3500 K. These simulations have shown that the foil damage with energies of 7 MeV/u and 10 MeV/u is very small.

Considering everything mentioned prior, it can be concluded that carbon foils are very applicable because they express considerable beneficial characteristics.

The foil should be placed after the injector linac or, if linac is made of two tanks then between the tanks.

A possibility of charge-exchange injection was investigated. In this case the damage of the foil and foil temperature remain low. The emittance blow up is about 18%.

Bibliography

[1] Amaldi U. History of hadrontherapy. Modern Physics Letters A. 2015;30(17):1540018.

[2] Peach K, Wilson P, Jones B. Accelerator science in medical physics. The British journal of radiology. 2011;84(special_issue_1):S4–S10.

[3] European Organization for Nuclear Research. Radiofrequency cavities; 2012. Available from: http://bit.ly/3bfUCm6.

[4] UCL Department of Physics and Astronomy. R-F Cavities; 2020. Available from: http://bit.ly/2SkGbog.

[5] CERN Accelerator School. Fifth general accelerator physics course. Turner S, editor. Geneve; 1994.

[6] Holzer B. Beam Dynamics in Synchrotrons. CERN Yellow Reports: School Proceedings. 2017;1.

[7] Marks N. Conventional Magnets for Accelerators; 2013. Available from: http://bit.ly/2S0JhPo.

[8] Amaldi U, Dosanjh M, Singers Sørensen B, Scholz M, Balosso J, Overgaard J, et al. CERN Yellow Reports: A facility for tumour therapy and biomedical research in South-Eastern Europe. CERN; 2019.

[9] Branlard E. Beam matrix and phase space; 2009. Available from: http://bit.ly/2Spccvo.

[10] Schaumann M. Particle Accelerators and Beam Dynamics: Part 3; 2019. Available from: http://bit.ly/39jYLUv.

[11] (CERN). MAD - Methodical Accelerator Design; 2019. Available from: http://madx.web.cern.ch/madx/.

[12] Syphers M. Particle Accelerators and Beam Optics; 2017. Available from: http://bit.ly/2v2JdWv.

[13] Courant ED, Livingston MS, Snyder HS. The strong-focusing synchroton—A new high energy accelerator. Physical Review. 1952;88(5):1190.

[14] Barton D, Beebe E, Gassner D, Grandinetti R, Hseuh H, Javidfar A, et al. Electron beam ion source pre-injector project (EBIS): Conceptual design report. Brookhaven National Laboratory; 2005.

[15] Zhao HW, Sun LT, Guo JW, Lu W, Xie DZ, Hitz D, et al. Intense highly charged ion beam production and operation with a superconducting electron cyclotron resonance ion source. Physical Review Accelerators and Beams. 2017;20(9):094801.

[16] Vretenar M. Linear Accelerators. Proceedings of the CAS-CERN Accelerator School: Advanced Accelerator Physics, Trondheim, Norway, 19–29 August 2013. 2014;.

[17] Hähnel H, Tiede R, Ratzinger U. Efficient Heavy Ion Acceleration with IH-Type Cavities for High Current Machines in the Energy Range up to 11.4 MeV/u. Proceedings of the 28th Linear Accelerator Conference 25–30 September 2016. 2017;.

[18] CERN. Accelerators; 2020. Available from: `https://home.cern/science/accelerators`.

[19] Manglunki D. Beam extraction. In: PS/SPS User Meeting; 2015. .

[20] Khan FM, Gibbons JP. Physics of radiation therapy. Lippincott, Williams & Wilkins; 2014.

[21] Samek D, Saračević L, Lagumdžija A. Fizika jonizirajućih zračenja. Veterinarski fakultet Univerziteta u Sarajevu; 2020.

[22] Garcia-Ramos JE, Alonso CE, Andres MV. Basic Concepts in Nuclear Physics: Theory, Experiments and Applications. Springer International Publishing; 2016.

[23] Gallant JL. Treatise on Heavy-Ion Science; 1985.

[24] Barth W, Fomichev A, Grigorenko L, Kulevoy T, Polozov S, Yaramyshev S. Charge stripping at high energy heavy ion Linacs. In: Journal of Physics: Conference Series. vol. 1350. IOP Publishing; 2019. p. 012096.

[25] National Electrostatics Corp . Gas and Foil Stripping; 2020. Available from: `http://bit.ly/2V3Yst0`.

[26] Ophel TR, Rhode A, Lobanov N, Weisser DC, Turkentine R, Wolf B, et al. Comparison of carbon stripper foils produced by arc discharge and laser ablation. Australian Institute of Nuclear Science and Engineering; 1998.

[27] Barth W, Clemente G, Dahl L, Gehard P, Groening L, Kaiser MS, et al. Carbon foil stripper tests with a high current uranium beam at 1.4 MeV/u. GSI, Darmstadt, Germany; 2010.

[28] Kupka K. Intense heavy ion beam-induced effects in carbon-based stripper foils [phdthesis]; 2016.

[29] Crawford HJ. Single electron attachment and stripping cross sections for relativistic heavy ions. University of California at Berkeley; 1979.

[30] Betz HD. Review of Stripping of Heavy Ions. Massachusetts Institute of Technology; 1971.

[31] INSP. ETACHA: a code to predict the charge-state distributions for multicharged ions in solids. Institut des Nanosciences de Paris; 2016.

[32] Lebedev SG, Lebedev AS. Calculation of the lifetimes of thin stripper targets under bombardment of intense pulsed ions. Institute for Nuclear Research of the Russian Academy of Sciences, Moscow, Russia Lomonosov Moscow State University, Faculty of Calculus Mathematics and Cybernetics, Moscow; 2008.

[33] Meroli S. Multiple scattering for particles in matter; 2012. Available from: `http://bit.ly/2SCjr4m`.

[34] Schardt D. Physical Characterization of Ion Beams in Radiotherapy, 2.1 Depth-Dose Profile (Bragg Curve). In: Hadrontherapy; 2019. .

[35] Cussol D. Nuclear Physics and Hadrontherapy; 2020. Available from: `http://bit.ly/3bSV4aq`.

[36] Hall EJ, Giaccia AJ. Radiobiology for the Radiologist. 7th ed. Lippincott Williams & Wilkins; 2012.

[37] Tang L, Wei F, Wu Y, He Y, Shi L, Xiong F, et al.. Role of metabolism in cancer cell radioresistance and radiosensitization methods; 2018. Available from: `https://jeccr.biomedcentral.com/articles/10.1186/s13046-018-0758-7`.

[38] Harada H. How Can We Overcome Tumor Hypoxia in Radiation Therapy. Radiation Research. 2011;.

[39] Taheri-Kadkhoda Z, Björk-Eriksson T, Nill S, Wilkens JJ, Oelfke JKA Uwe, Huber PE, et al. Intensity-modulated radiotherapy of nasopharyngeal carcinoma: A comparative treatment planning study of photons and protons. 2008;.

[40] Hirohiko T, Tadashi K, Toshiyuki N Shirai Koji, Hiroshi T, Kumiko K. Carbon-Ion Radiotherapy. Springer-Verlag GmbH; 2013. Available from: `https://www.ebook.de/de/product/22281890/carbon_ion_radiotherapy.html`.

[41] IAEA. Radiation Oncology Physics: A Handbook for Teachers and Students. Podgorsak EB, editor; 2005.